ELSEVIER

Contents lists available at ScienceDirect

Structural Safety

journal homepage: www.elsevier.com/locate/strusafe





Models and methods for probabilistic safety assessment of steel structures subject to fatigue

Johan Maljaars ^{a,b}, John Leander ^c, Alain Nussbaumer ^d, John Daalsgaard Sørensen ^e, Daniel Straub ^{f,*}

- a Department Reliable Structures, TNO, The Netherlands
- ^b Department Structural Engineering and Design, Eindhoven University of Technology, The Netherlands
- ^c Div. Structural Engineering and Bridges, KTH Royal Institute of Technology, Sweden
- ^d ENAC-RESSLab, Ecole Polytechnique Fédérale de Lausanne, Switzerland
- e Department Civil Engineering, Aalborg University, Denmark
- f Engineering Risk Analysis Group, Technical University of Munich, Germany

ARTICLE INFO

Keywords: Fatigue Fracture Reliability Inspections Steel structures

ABSTRACT

We review of the state of the art in probabilistic modelling for fatigue reliability of civil engineering and offshore structures. The modelling of randomness and uncertainty in fatigue resistance and fatigue load variables are presented in some detail. This is followed by a review of the specifics of reliability analysis for fatigue limit states and a background on the semi-probabilistic treatment of fatigue safety. We discuss the different life-cycle reliability concepts and give an overview on probabilistic inspection planning. We describe the choices made in the Probabilistic Model Code of the Joint Committee of Structural Safety, present alternatives to these choices and suggest areas of future research.

1. Introduction

The development of local material damage caused by fluctuating actions, known as fatigue, is one of the most important failure modes of many structural materials. Wöhler's study into fatigue failure of rail wheels [1] is the first known systematic study into the phenomenon. Since then, fatigue has been an area of extensive research and development, with many lessons learned from failures in practice. While fatigue is of particular concern in moving structures, such as ships, trains, aircrafts and engines, it can also lead to catastrophic failures in civil engineering and offshore structures. Fatigue cracks in metallic structures are typically observed at spots where high local stresses and stress fluctuations are accompanied by metallurgical imperfections. This makes welded, but also riveted and bolted, joints most prone to fatigue failure.

The first major collapse of a bridge for which fatigue was identified as the probable cause took place in 1876 [2], but it was only between 1930 and 1960 that bridge engineers started to realize that the large number of heavy axles crossing bridges required consideration in the design. Studies of bridge failures indicate that fatigue is one of the major sources of damage and collapse in these structures [3,4]. The fatigue-induced total collapse of the Norwegian semi-submersible drilling rig "Alexander L. Kielland" highlighted the susceptibility of

civil offshore structures to fatigue [5]. (On- and offshore) wind turbine support structures are a more recent type of structure heavily loaded by fatigue [6], with a significantly different fluctuating load effect than other civil engineering structures. Crane runways represent another example of civil engineering structures subject to cyclic loading and fatigue [7,8].

Fatigue is a highly random process, in which all phases (crack initiation, propagation, and fracture) are subject to significant aleatory and epistemic uncertainty. On the one hand, these uncertainties relate to the material and resistance properties, such as fatigue crack growth rates, geometrical stress concentrations and metallurgical flaws. The applied fatigue models are simplified and based on empirical correlations, which leads to significant uncertainty in the prediction of the fatigue strength. This motivates the use of a probabilistic description of fatigue strength. On the other hand, actions and action effects are subject to scatter and uncertainty. In contrast to other failure modes, for fatigue it is not only the extreme value but the entire load history that is relevant and specific fatigue load models are applied.

Because of the random nature of resistance and action and the associated large uncertainties, probabilistic fatigue assessment is common in research and some industries. Following probabilistic studies into fatigue of aluminium airplanes in the 1960s, the first probabilistic

E-mail address: straub@tum.de (D. Straub).

^{*} Corresponding author.

analyses of welded steel motorway bridges and offshore structures appeared in the 1970s and early 1980s [9–11]. These studies evaluated the entire life of structures. Studies into the remaining life of civil and offshore structures, considering the effect of inspections, appeared in the late 1980s [12], followed by risk-based inspection planning for fatigue [13–15]. The possibilities of monitoring load effects have increased tremendously over the years and these have been included in probabilistic fatigue life studies [16–18]. Throughout all these years, the models for fatigue resistance and fatigue loads have been refined and this is a continuous process to-date.

The importance of fatigue failures and the large uncertainties associated with their prediction have also motivated the structural reliability community, including the Joint Committee on Structural Safety (JCSS), to develop probabilistic models and tailored reliability analysis tools (e.g., [19–24]). Section 3.12 of the JCSS Probabilistic Model Code [25] is devoted to fatigue and summarizes the two most common approaches to fatigue reliability assessment, the S-N model (see Sections 2.1–2.2) and the model based on Fracture Mechanics (FM), (see Section 2.3).

This paper gives an overview on the background and the current state of the art in probabilistic models and reliability assessment for fatigue life and fatigue growth predictions in civil engineering steel structures, with an emphasis on welded joints because of their sensitivity to fatigue (Section 2), probabilistic models describing fatigue loads (Section 3), as well as the treatment of uncertainties in a semi-probabilistic design (Section 5) and life-cycle management (Section 6). The overview includes generally used distributions of the relevant random variables. Consequences of the selection of probabilistic models are highlighted and knowledge gaps and areas of future research identified.

2. Probabilistic fatigue resistance models

2.1. The S-N curve model for constant amplitude load

The modelling of fatigue resistance is largely based on empirical evidence. Theoretical models are employed for qualitative relationships and understanding, but fatigue tests are employed to quantify these relationships. The basic type of fatigue experiment has the geometry, the stress range Δs and the stress ratio $R = s_{min}/s_{max}$ as independent variables and the applied number of cycles N (if possible until failure, in which case called the fatigue life) as dependent variable. In this setting, the fatigue life is subject to significant scatter. In contrast to mechanically fastened connections and casted components, R is generally considered unimportant for welded connections because of the residual stress caused by the welding process, even though it does influence the fatigue life to some extent for small specimens [26]. The stress ratio effect is therefore usually ignored in (probabilistic) evaluations of welded connections. Various methods are available to statistically evaluate fatigue life data [27]. The Basquin relation [28] is the most widely used relation to describe the outcomes of high cycle fatigue tests of welded connections:

$$N = K_1 \Delta s^{-m_1} \tag{1}$$

The exponent parameter m_1 is modelled deterministically, either as learned via a maximum likelihood estimate from the test data or based on (fully informative) prior information from large test databases of (other) welded joints, giving $m_1 = 3$. The uncertainty is expressed by modelling K_1 as a random variable, whereby K_1 is often assumed to be lognormal, sometimes Weibull distributed [29,30], also multimodal distributions are considered [31]. Even though better methods are available (see below), it is common practice to ignore tests terminated without failure, so-called run-outs.

As an example of the scatter in typical fatigue tests, Fig. 1(a) provides a collection of fatigue test data from literature consisting of 87 series, where each black circle represents a specimen tested to

failure (1477 tests) and each red triangle represents a run-out (249 tests). All specimens consist of a loaded plate or section with as-welded (i.e. no post weld treatment) single or double sided transverse non-load carrying attachments with a weld-toe-to-weld-toe-distance $L \leq 50$ mm and all tests are carried out with a low minimum stress ($0 \leq R \leq 0.2$). The data are taken from collective reports and papers [32–37] (the latter excluding tests on beams) and from documents published since 1955 for Commission XIII of the International Institute of Welding. Using the fixed value $m_1 = 3$ and a lognormal distribution for K_1 , the mean of the 10-base logarithm of K_1 , $\log_{10}(K_1)$, is $\mu_{\log(K1)} = 12.54$ and its standard deviation is $\sigma_{\log(K1)} = 0.30$. This standard deviation is substantial, even though the geometry of this type of detail is well defined; e.g., it does not contain axial misalignment.

The standard deviation $\sigma_{\log(K1)}$ is actually a function of the stress range. To demonstrate this, Fig. 1(b) gives the standard deviation evaluated at certain tested stress ranges, each data point evaluated using at least 3 series and 15 tests. The data points are limited to stress ranges of $\Delta s > 180$ MPa so that the run-outs do not influence the results. The results are obviously subject to scatter, but the trendline of the data indicates a decreasing standard deviation with increasing stress range. This trend is observed also for other types of detail (including non-welded details, [29]) but it is ignored in the simple Basquin equation.

The parameters $\mu_{\log(K1)}$ and $\sigma_{\log(K1)}$ are evaluated per series for the same test data. The standard deviation of all values of $\mu_{\log(K1)}$ is equal to 0.27, i.e., the difference between the individual test series is substantial, attributed to differences in weld quality, material, geometry and test facilities. The average value of all values of $\sigma_{\log(K1)}$ is 0.15 and its standard deviation is 0.08, showing that the uncertainty per series is substantially smaller than that of the entire database. The lesson is that probabilistic fatigue analyses should be based on test databases containing a sufficient number of individual test series. One can make use of the data of individual test series if a structure is considered that contains multiple details of the same type. In a system analysis, a mean per test series $\mu_{\log(K1)}$ can be randomly selected using the expectation of 12.54 and the standard error of 0.27 and the standard deviation $\sigma_{\log(K1)}$ can be selected using the expectation of 0.15 and the standard error of 0.08

The mean, but also the standard deviation of $\log_{10}(K1)$ are detail dependent. The standard deviation of welded details is reported to range between $0.18 \leq \sigma_{\log(K1)} \leq 0.25$ [38,39] or $0.1 \leq \sigma_{\log(K1)} \leq 0.22$ [40], the latter based on a limited number of tests. More recent re-evaluations of large databases for an update of the standard EN 1993-1-9 [41] generally gave larger standard deviations [42]. The often used value $\sigma_{\log(K1)} = 0.2$ [25,43] might therefore be too generic. For example, the standard deviation of bolts in tension with rolled thread ranges between $0.15 \leq \sigma_{\log(K1)} \leq 0.18$ and that of bolted joints with cover plates ranges between $0.24 \leq \sigma_{\log(K1)} \leq 0.53$ for tests with $0 \leq R \leq 0.1$ [44].

A single Basquin relation no longer applies in case of relatively low stress ranges. A transition takes place from surface to subsurface crack initiation, with a resulting larger initiation life and an associated larger value of m_1 . This effect is highly dependent on the material type, the environment and the surface condition and therefore highly uncertain for general applications [45,46]. However, due to the very high number of applied cycles required for failure, this second part of the dual slope S-N curve is often irrelevant for civil engineering and it may then be convenient to assume a Constant Amplitude Fatigue Limit (CAFL) Δs_0 below which an infinite life applies. A lognormal distribution is usually assumed for Δs_0 [47] and the maximum likelihood method is used to derive the distribution parameters, using both failed data and run-outs. A number of models exist that describe the finite life fatigue resistance as conditional to the CAFL [47–50]. These so-called random fatigue limit models use the following general expressions. The

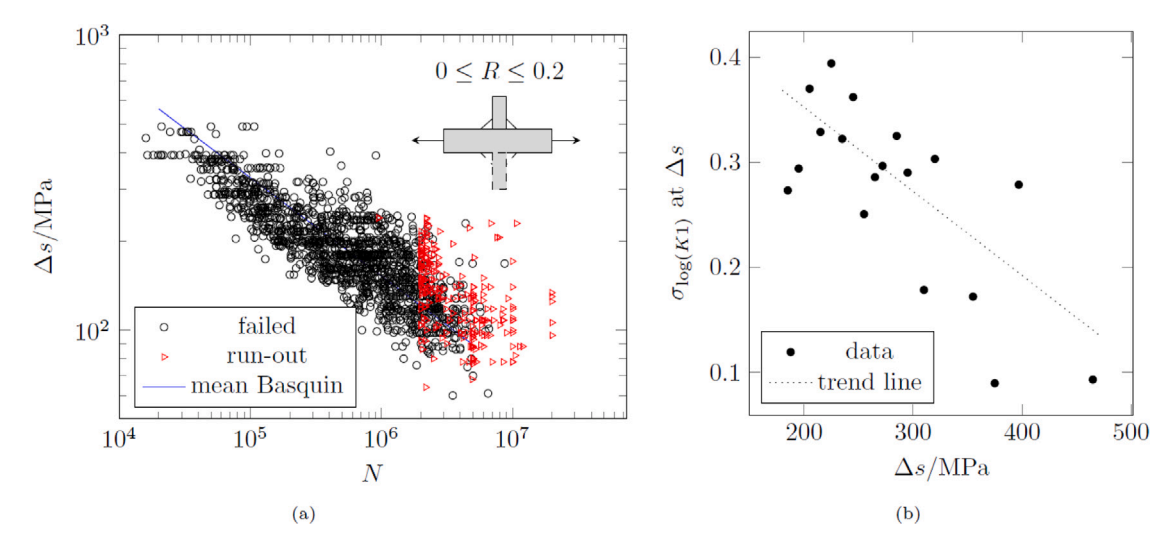


Fig. 1. Fatigue of welded transverse attachment with L < 50 mm and $0 \le R \le 0.2$: (a) Test data; (b) Standard deviation of fatigue life (logarithm) at the indicated stress range.

Probability Density Function (PDF) of the 10-base logarithm of the CAFL $v = \log_{10} \left(\Delta s_0 \right)$ is:

$$f_v(v) = \frac{1}{\sigma_v} \phi\left(\frac{v - \mu_v}{\sigma_v}\right) \tag{2}$$

where ϕ is the PDF of the standard normal distribution and σ_v is the standard deviation of the CAFL. The PDF of the conditional probability of the finite fatigue life (for Δ $s > \Delta$ s_0) is:

$$f_{w|v}(w|v) = \frac{1}{\sigma_{w|v}} \phi\left(\frac{w - \mu_w}{\sigma_{w|v}}\right)$$
(3)

where $w=\log_{10}\left(N\right)$ with its mean μ_w given by the S-N curve (e.g., in case of the Basquin relation, $\mu_w=\log_{10}(K_1)-m_1\log_{10}(\Delta s)$) and its standard deviation conditional to the fatigue limit $\sigma_{w|v}$. The marginal PDF of the fatigue life is:

$$f_{w}(w) = \int_{-\infty}^{\log_{10}(\Delta s)} f_{w|v}(w|v) f_{v}(v) dv$$
 (4)

The model parameters are inferred using the maximum likelihood method, see [47]. This allows to include information from run-outs and to account for the scatter in the CAFL. The model proposed in [50] can account for the smaller scatter of the fatigue resistance at higher stress range levels, and/or a more gradual transition between the finite life and the CAFL, resulting generally in a substantially better performance compared to the Basquin relation according to Akaike Information Criterion (AIC) scores [51]. In contrast, the advantage of the Basquin relation is its simplicity.

2.2. The S-N curve extension for variable amplitude load

The S-N curve is known to change if the detail is subjected to variable amplitude load and the fatigue propagation life dominates the entire fatigue life, which is the case for welded joints. A dual slope S-N curve results if a fraction of the load spectrum contains stress ranges exceeding the CAFL. Using the Basquin relation:

$$N = K_2 \Delta s^{-m_2} \text{ for } \Delta s \le \Delta s_0$$
 (5)

and Eq. (1) applies to stress ranges $\Delta s > \Delta s_0$. This change in S-N curve can be explained with the principals of FM: the cycles above the CAFL cause a small crack to initiate so that also stress ranges just below the CAFL contribute to crack growth. The more cycles applied, the larger the crack grows, the more severe is the stress intensity field near the crack tip and the larger is the fraction of the load spectrum that contributes to further crack growth. The associated slope parameter m_2 is larger than m_1 but smaller than the slope parameter associated

with the near infinite life regime under constant amplitude load. As a convention, the parameter m_2 is often taken as $m_2 = m_1 + 2$ or as $2m_1-1$ as proposed by Haibach [52,53], but FM principles indicate (and tests confirm) that it actually depends on the shape of the spectrum, the fraction of cycles above the CAFL and the type of detail. Only few data are available from which the fraction of cycles above the CAFL can be estimated that result in the change from a single to a dual slope S-N curve, but the fraction appears very small [54].

The most commonly used assumption with the Basquin relation is a fixed value of the number of cycles at the CAFL, and full correlation between the two slopes, so that K_2 follows from K_1 . Such a description is applied in the Probabilistic Model Code [25]. However, because of the limited test data available to evaluate the parameters K_2 and m_2 , their values are subject to significant epistemic uncertainty. This is sometimes taken into account by assuming $\sigma_{\log(K2)} > \sigma_{\log(K1)}$ [55]. One could consider the increased uncertainty for larger number of cycles (smaller stress ranges) by taking slope parameter m_2 as a random variable.

The description of this S-N curve is accompanied by the linear damage accumulation assumption by Palmgren and Miner [56,57]:

$$D(\mathbf{X},t) = \sum_{\text{all cycles up to } t} \frac{1}{N_i(\mathbf{X})}$$
 (6)

where D is the damage measure, $N_i(\mathbf{X})$ is the fatigue life for each applied stress range Δs_i in the spectrum. It is a function of random model parameters \mathbf{X} and determined using Eqs. (1) and (5). The limit state function is:

$$g(\mathbf{X},t) = D_{lim} - D(\mathbf{X},t) \tag{7}$$

where **X** is the vector of random variables, t is the time, and D_{lim} is a random variable indicating the damage at which failure of the detail occurs. A lognormal distribution is often assumed for D_{lim} with a mean of $\mu_{Dlim}=1$ and a standard deviation of $\sigma_{Dlim}=0.3$. This distribution is attributed to Wirsching [58] and probably based on the experiments in [57]. It should be noted that the distribution of D_{lim} is correlated to the choice of the S-N curve with associated parameters s_0 , m_2 and $\sigma_{log(K2)}$. The distribution of D_{lim} implicitly contains the retarding and accelerating effects of load sequence and it thus depends on the load history.

The previous description makes clear that the extended S-N curve is largely based on conventions, but it is simple in use and appears to give results in reasonable agreement with test data. Some probabilistic descriptions of the variable amplitude S-N curve exist that take account of the uncertainty in m_2 and the number of cycles above the CAFL, by considering a gradual transition from the constant amplitude S-N curve

to the variable amplitude S-N curve [59–61]. In these models, the CAFL is replaced by a fatigue threshold that is equal to the CAFL in absence of damage and that gradually drops as the damage applied increases.

2.3. Fatigue fracture mechanics

Fatigue FM makes use of the empirical correlation between the crack growth rate, i.e., the average crack extension per cycle da/dN and the stress intensity factor range ΔK . Although a debate exists on the theoretical soundness of the similitude concept of ΔK [62], the correlation has shown to be a convenient tool for evaluating the crack propagation life for engineering purposes. The stress intensity factor range is originally developed for cracks with a straight crack front:

$$\Delta K = Y \Delta s \sqrt{\pi a} \tag{8}$$

where a is the crack size and Y is a geometric correction factor, explained later.

Surface cracks in real structures are usually modelled as having a semi-elliptical shape. In such a case, two coupled equations are used to describe the crack extension in depth and in surface direction. The associated stress intensity factors are defined as, respectively, [63,64]:

$$\Delta K_a = Y_a \Delta s \sqrt{\pi a} \tag{9}$$

$$\Delta K_c = Y_c \Delta s \sqrt{\pi a} \tag{10}$$

where parameters Y_a and Y_c are a function of the crack dimensions – expressed through the semi-elliptical crack depth a and semi surface length c – the local geometry and the loading mode. These parameters can be obtained with the finite element method, alternatively parameterized equations from the literature based on the finite element method can be used.

Various fits of crack growth experiments are used in the literature to correlate da/dN with ΔK , e.g. [64,65]. In the most simple shape, for steels in air:

$$da/dN = \begin{cases} C\Delta K^p & \Delta K > \Delta K_{th} \\ 0 & \Delta K \leq \Delta K_{th} \end{cases} \tag{11}$$

A strong correlation exists between parameters p and C [66]. In practical assessments, a fixed (deterministic) value is often considered for p and the variability in the crack growth experiments is expressed through a lognormal distribution of C. For p selected as 3, a expressed in [mm] and ΔK expressed in [N/mm^{3/2}], the 10th base logarithm of C has a mean equal to $\mu_{log(C)} = -12.74$ and a standard deviation of $\sigma_{log(C)} = 0.11$ or 0.22 for base metal and weld metal, respectively [43]. The values apply for the as-welded condition, assuming high tensile residual stresses and hence a high stress ratio. The Probabilistic Model Code [25] uses an alternative, 2-stage relation for Eq. (11) with variable distributions taken from [64]. The crack propagation rate C varies within a specimen and can hence also be modelled as a stochastic process [67]. The fatigue growth threshold ΔK_{th} , below which crack growth does not occur, depends on many factors, including the corrosivity of the environment, the crack size [68], the stress ratio [69] and microstructural properties, usually considered by hardness [70]. As a simplified approximation for high stress ratios, BS 7910 [64] gives a characteristic value equal to 2 MPa \sqrt{m} = 63 N/mm^{3/2}, a scatter related to test reproducibility of 10% (5% from the mean) and an additional scatter of 10% for different batches of material for ΔK_{th} . This could be interpreted as a mean and a standard deviation of the threshold of $\mu_{Kth} = 2.5 \text{ MPa} \sqrt{\text{m}}$ and $\sigma_{Kth} = 0.25 \text{ MPa} \sqrt{\text{m}}$, respectively. The Probabilistic Model Code [25] provides a much higher mean and coefficient of variation ($\mu_{Kth} = 4.4 \text{ MPa}\sqrt{\text{m}}$ and $\sigma_{Kth} = 1.8 \text{ MPa}\sqrt{\text{m}}$); the difference is caused by different test conditions (stress ratio, crack size). The model in [25,64] is a gross approximation of the actual complex condition. The threshold condition and the transition from

the threshold to the propagation stage are important for an accurate fatigue life prediction and they are the subject of recent and ongoing studies [69,71–75]. Note that a similar expression as Eq. (11) applies in surface (c) direction of the crack.

2.4. Initial crack size

For simulation of the entire crack propagation stage in welded joints, Eq. (11) is integrated starting from an initial crack size a_0 . This size is usually calibrated with FM simulations instead of measured crack sizes, because of different sharpness of initial flaws (e.g., undercut [76]) and because the probabilistic FM formulation considers a single crack, whereas multiple cracks along the weld toe or root initiate in reality and these coalesce to a dominant crack after a certain growth period. Based on [77], the equivalent initial flaw size is lognormal distributed in the Probabilistic Model Code [25], with a mean depth of μ_{a0} = 0.15 mm and a standard deviation of $\sigma_{a0} = 0.10$ mm and it has a lognormally distributed aspect ratio with a mean of $\mu_{a0/c0} = 0.62$ and a standard deviation of $\sigma_{a0/c0} = 0.25$. Other distribution parameters used by many are proposed in [78,79], see also [80]. The initial crack size and the radius at the weld toe ρ – the transition between the weld and the base metal - appear the two most influential variables for the fatigue life, [78]. The latter variable is described with a Weibull distribution [78] with a mean that varies among test series, ranging from around 0.5 mm to 2.5 mm and a coefficient of variation (CoV) of 0.5 to 1 [76,78,81-84]. The importance of these variables implies that the fatigue life strongly depends on the weld quality, which corresponds with experimental findings.

However, fatigue FM is especially suited for estimating the structural reliability in case fatigue prone details are subjected to (periodic) fatigue inspections. This is elaborated in Section 5.2.

2.5. Fracture

As the crack size increases, the weakened structure may approach a condition of unstable crack growth when subject to a relatively high load. Since the vast majority of the entire fatigue life is in the initiation and growth of small cracks, the crack size at unstable crack growth is of limited importance for modelling the entire fatigue life. This is also the reason why the unstable crack growth condition is not considered in the S-N model of Section 2.1, provided that the material satisfies a certain, minimum fracture toughness checked by Charpy-V tests. Parametric equations for K, e.g. those in [63], are often valid up to 0.8 times the component thickness. In such a case, the limit state equation can be approximated as:

$$g(\mathbf{X},t) = 0.8B - a(\mathbf{X},t) \tag{12}$$

where B is the component thickness.

However, the unstable crack growth condition may be important for:

- Relatively brittle steels, such as old steels produced with the Thomas process or very high strength steels, Fig. 2(a): the life of a brittle steel N_b may be substantially shorter than that of a tough steel N_p.
- Large components in realistic structures, which may exhibit a
 lower crack growth rate at large crack sizes as compared to small
 specimens, Fig. 2(b): the influence of the fracture toughness on
 the life of the large component N_I is larger than that of the small
 specimen N_c.
- Details for which the structural integrity relies on fatigue inspections, Fig. 2(c): the fracture toughness is relatively important for the remaining life after detection (N₁ N_d and N₂ N_d), or the detectable crack size a_d may even be larger than the critical crack size.

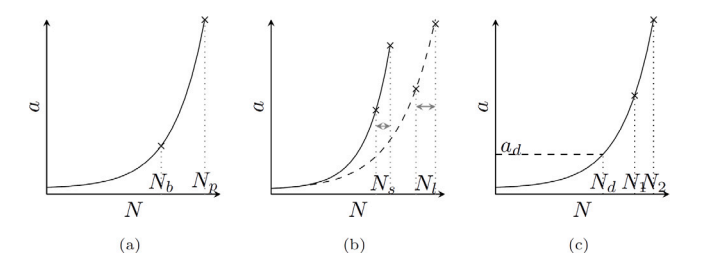


Fig. 2. Schematic crack growth curves with crack size a versus number of cycles N. Crosses represent failure: (a) A brittle steel with life N_b and a tough steel with life N_g ; (b) A small specimen with life N_s and a large component with life N_l ; (c) Life of two steels N_1 and N_2 and elapsed life after possible detection N_d at detectable crack size a_d .

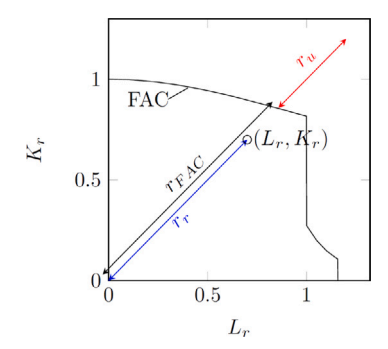


Fig. 3. Failure assessment line (example for a material with yield plateau).

The unstable crack growth condition is represented by a Failure Assessment Curve (FAC, Fig. 3), which depends on the stress–strain relationship and the crack tip constraint [85]. The curve describes the interaction between plastic failure, represented by a plasticity ratio L_R , and (brittle) fracture, represented by a fracture ratio K_R . In its most simple form:

$$L_R = s_{ref}/s_v \tag{13}$$

$$K_R = K/K_{mat} + \rho \tag{14}$$

where s_{ref} is the stress in the remaining ligament, s_y is the yield stress, K is the stress intensity factor (using Eq. (8) but with Δs replaced by the maximum stress), K_{mat} is the fracture toughness and ρ is an interaction factor. As the crack grows, s_{ref} and K increase. The crack is "safe" against unstable crack growth as long as the assessment point (L_r, K_r) remains within the FAC. In probabilistic assessments, an additive model uncertainty factor r_u applies to the FAC [86]. The limit state function is:

$$g(\mathbf{X},t) = r_{FAC} + r_u - r_r(\mathbf{X},t)$$
(15)

where r_r is the radial distances of the assessment point (L_r,K_r) and r_{FAC} is the radial distance to the FAC for the same polar coordinate (Fig. 3). A lognormal distribution applies to r_u , with distribution parameters depending on the choices made in the fracture evaluation, with models and values given in [87], based on comparisons with wide plate and tubular joint tests. Note that the Probabilistic Model Code [25] uses another model to express the uncertainty in the FAC than Eq. (eq:limFM), but that model is based on a small part of the test database in [87] and it cannot be used in combination with more recently developed alternatives for the FAC description. The probabilistic fatigue life can be determined by integrating Eq. (11) up to the point where the combination (L_r,K_r) is such that the limit state is reached.

2.6. Variable amplitude FM

In case of an ergodic variable amplitude load spectrum, the rate da/dN can be determined at each crack increment as the average growth rate over all individual cycles. Load sequence effects [88] and crack retardation and acceleration [89] are ignored in this case. It would then be appropriate to add an uncertainty factor u (although – to the knowledge of the authors – such a factor has not been applied hitherto):

$$da/dN_{average} = \frac{1}{u \cdot n} \sum da/dN_i$$
 (16)

where $i \in (1 \dots n)$ is an applied cycle with corresponding stress intensity factor range ΔK_i and crack growth rate da/dN_i following Eq. (11) and u is an uncertainty factor for which, equivalent to the critical damage parameter in Eq. (7), a lognormal distribution can be assumed with mean $\mu_u = 1$ and standard deviation $\sigma_u = 0.3$.

2.7. Compatibility between the S-N model and the FM model

Ample studies report on the consistency between the probabilistic S-N model and the probabilistic FM model, e.g. [90–93]. The studies generally conclude that similar reliability levels are obtained with the two models, sometimes after calibration of some distributions of variables, such as the initial crack size representative for the as-welded stage in the FM model, or the slope parameter m_2 of the S-N model. The similarity in results is important, since it implies that either probabilistic model can be adopted in practical assessments and they are therefore both included in the Probabilistic Model Code [25].

Fig. 4 compares the results of the FM model to the test database of Fig. 1, using Eqs. (9)–(12), where Y_a and Y_c are composed of the product of the elliptical surface crack correction factors in [63], the 3D weld toe notch radius correction factor of [94] and correction factors for the weld toe radius ρ and the weld flank angle θ of [95]. The black dots in Fig. 4(a) give the ratio between the FM prediction N_{FM} and the tested number of cycles N_{exp} of each individual test, using median values of the FM variables as given above.

The bias of the prediction, expressed as the mean of $(\log_{10}(N_{FM}) \log_{10}(N_{exp})$, is equal to -0.10, i.e. the average predicted life is a bit lower than the average life of the tests. This can be explained by the stress ratio effect in small welded specimens [96]: The value for C in Eq. (11) is derived for R = 0.5 whereas the specimens were tested at $0 \le R \le 0.2$. The scatter, expressed by the standard deviation of $(\log_{10}(N_{FM}) - \log_{10}(N_{exp}))$, is 0.28, i.e. similar to $\sigma_{\log(K1)}$ of the Basquin fit, even though the difference between the S-N and the FM models of some individual series is large. The latter is attributed to the specimen dimensions and loading mode (tension or bending) being parameters explicitly accounted for in the FM simulation, Fig. 4(b). The local weld geometry variables ρ and θ were measured in some of the test series. These tests are re-evaluated with the reported average values per series of ρ and θ (blue dots in Fig. 4(a)), causing a slight reduction of the standard deviation. The limit state of Eq. (12) is also evaluated using the reported distributions of the variables using Monte Carlo simulation, for a plate of 10 mm thickness loaded in tension with a distance between the weld toes of the attachment of 20 mm. The standard deviation of the 10th base logarithm of the predicted number of cycles according to this model is 0.12, comparable to the average experimental scatter per test series (i.e. per geometry) of 0.15 (Section 2.1).

Table 1 summarizes the distributions of the fatigue resistance random variables discussed in this section. It gives alternatives to the distributions currently included in the Probabilistic Model Code [20]. The table is not intended as a complete overview of all possible alternatives put forward in the literature.

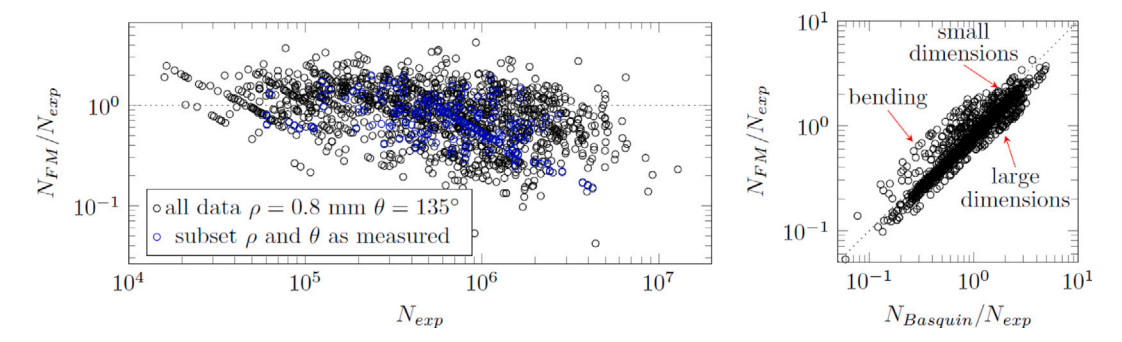


Fig. 4. Fracture mechanics simulations versus test data of Fig. 1: (a) Compared to test data; (b) Compared to Basquin fit. (For interpretation of the references to colour in this figure legend, the reader is referred to the web version of this article.)

Table 1
Possible distributions for fatigue resistance variables (units: N, mm).

Description	Symbol	Distribution	Mean	CoV	Source
Basquin slope parameters ^a	m_1 and m_2	Deterministic	3 and 5	-	[25]
Basquin constant ^a	K_1	Lognormal or Weibull	Detail dependent ^b		[39]
Basquin constant ^a	K_2	Lognormal or Weibull	Fully correlated to K_1^c		[25]
Damage at failure	D_{lim}	Lognormal	1	0.3	[58]
Crack growth exponent	р	Deterministic	3 ^d	-	[43]
Crack growth rated	C	Lognormal	$1.8 \cdot 10^{-13}$	0.11 - 0.22	[43]
Crack growth threshold ^e	ΔK_{th}	Lognormal	79	0.1	[64]
		Lognormal	140	0.4	[25]
As-welded crack depth	a_0	Lognormal	0.15	0.66	[77]
As-welded crack aspect ratio	a_0/c_0	Lognormal	0.62	0.40	[77]
Weld toe radiusf	ρ	Weibull	0.5-2.5	0.5-1.0	Section 2.3
Load sequence uncertainty ^f	и	Lognormal	1	0.3	Section 2.3
FAC uncertainty ^g	r_u	Lognormal	1.09-1.46	0.14-0.37	[87]

- a AIC scores indicate that random fatigue limit models generally better describe test data than the Basquin equation used in [25].
- b Based on [97], a CoV of 0.2 is assumed in [25]. Detail class dependent values in [39].
- ^c Larger uncertainty of the second stage can be considered through a larger CoV for K_2 or taking m_2 as random variable.
- ^d Based on [64], a two-stage curve is used in [25].
- $^{\rm e}$ It is better to formulate ΔK_{th} as stress ratio and crack size dependent, Section 2.3.
- f Important variable, but not considered in [25].
- g An alternative, but outdated, FAC description is given in [25].

3. Fatigue loading

Fatigue deterioration is driven by loads varying over time such as fluctuating environmental loads and moving vehicles. They are inherently associated with high uncertainties that need to be modelled in a probabilistic analysis. The load descriptions in this section are aimed at large civil engineering structures, such as bridges, offshore structures, and support structures to wind turbines, subjected to variable amplitude loading and a high number of cycles during the service life.

Following Section 2.1, the decisive load effect is the stress range and the associated number of cycles, for some fatigue models complemented with stress ratio or maximum stress. The load effect for a specific structural detail is typically represented by a stress range spectrum reflecting the distribution of stress ranges and the associated number of cycles. For illustration, an example empirical spectrum is shown in Fig. 5 with stress ranges between 10 MPa and 60 MPa, as a conventional histogram in (a) and the same distribution as an accumulated spectrum in (b), with $N_{\rm T}$ as the total number of cycles.

The distribution of stress ranges exemplified by Fig. 5 depends on the loading scenario and the structural response. It should be noted that the distribution can be discontinuous and multimodal over the stress ranges. Possible reasons are scattered loading or complex structural response caused by interactions, transients, dynamics, damping, and non-linear behaviour. Some publications suggest a simplification of the stress range spectrum to a damage equivalent stress range defined

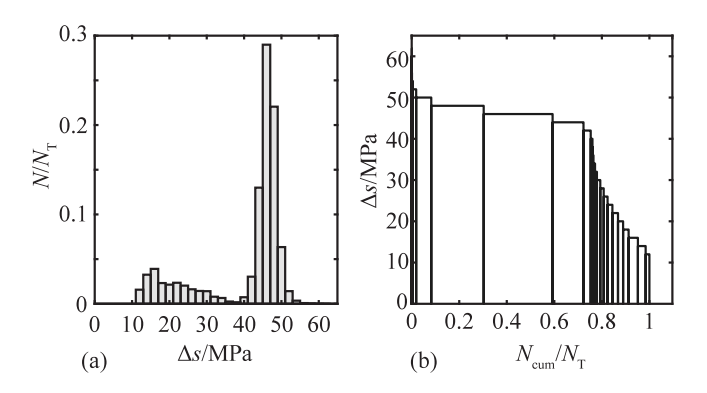


Fig. 5. An example empirical stress range spectrum shown as (a) a histogram and (b) an accumulated spectrum.

as [10]:

$$\Delta s_{\rm eq} = \left(\frac{1}{N_{\rm T}} \sum_{i=1}^{N_{\rm T}} N_i \Delta s_i^m\right)^{1/m} \tag{17}$$

which is valid for a single slope S-N curve with slope parameter m. This reduces the spectrum to a single value which inevitably discards information about the distribution of stress ranges. This would allow to express the limit state function in terms of stress range instead of damage as per Eq. (7). However, with the fatigue strength described

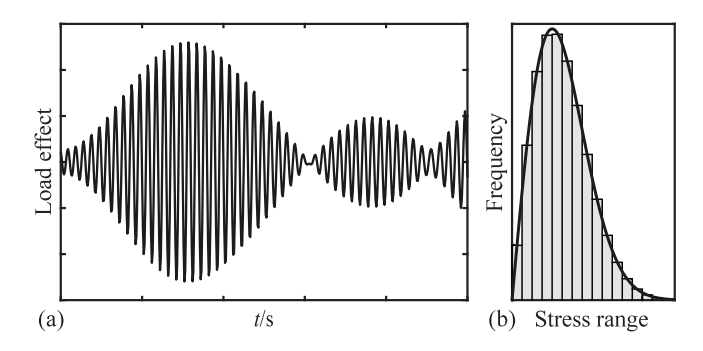


Fig. 6. A narrowband Gaussian stochastic process realization as a time series (a) and a resulting Rayleigh distributed stress range spectrum (b).

considering threshold levels and bilinear curves, it is advisable to consider the complete spectrum distribution [98].

As basis for a probabilistic analysis, stress range spectra may be attained by [99]

- 1. spectral analysis (linear); or
- 2. time domain analysis (linear or non-linear).

Analytical solutions based on idealized loading are utilized in spectral analyses. A typical case is a narrowband Gaussian stochastic process giving a Rayleigh distribution of stress ranges [100,101], see Section 3.1.1. Spectral analyses are relevant, e.g., for wave loading on floating structures [99,102] and described as simplified fatigue analysis in [97].

Time domain analyses build upon generated time histories of stresses and cycle counting. The rainflow counting method is the most common, attributed to Matsuishi and Endo [103] and described as a standardized method in regulations [104,105].

The Probabilistic Model Code [25] provides model uncertainty factors associated with calculating load effects, but does not cover probabilistic load models for fatigue. However, such load models are available and are summarized in the following.

3.1. Models for wind and wave loaded structures

Wind and waves are environmental actions regarded as stochastic processes, described by power spectral densities (PSDs). The following descriptions are limited to wind speed and wave height, which are decisive for fatigue deterioration. For a detailed probabilistic assessment, loads associated to all possible operational scenarios should be considered, see e.g. [106] for more details.

The structural analyses that are required for attaining the load effect, as stresses and stress range spectra at the studied details, are not described here. These typically involve case-specific advanced dynamic models considering aerodynamics, hydrodynamics, coupled analyses, and control systems [99].

3.1.1. Narrowband stochastic processes

A narrowbanded stochastic process can be described as an approximation of a harmonic function with a fixed single frequency [101]. Others have described it as a function with one single peak following each zero crossing [9]. Mathematical definitions can be found in [101]. An example of a simulated narrowband Gaussian process is shown in Fig. 6(a) as a time series. It reflects an oscillation with fixed frequency but varying heights of the peaks.

If the stress history at a specific point in a structure is narrowbanded and Gaussian, the resulting stress range spectrum follows a Rayleigh distribution as shown in Fig. 6(b). Moreover, a closed mathematical expression is available for the expected stress range (to the power m) [100]:

$$E\left[\Delta s^{m}\right] = \left(2\sqrt{2}\,\sigma\right)^{m}\Gamma\left(\frac{m}{2} + 1\right) \tag{18}$$

where m is the slope parameter of the single slope S-N curve or crack growth rate curve, σ is the standard deviation of the stress process, and $\Gamma(\cdot)$ is the Gamma function. Eq. (18) is valid for a constant slope m. For threshold values and bilinear curves, incomplete Gamma functions can be used for the different branches, as summarized in the Probabilistic Model Code [25].

3.1.2. Wave loading

Waves are produced by wind, with higher wind speeds leading to larger waves. For the assessment of an offshore structure, the waves produced by a given wind speed are needed, which are determined from idealized PSDs. The narrowband approximation in Section 3.1.1 can be appropriate for simplified fatigue assessments [97]. Measurements have shown, however, that wave loading has contributions from a broad band of frequencies, making time domain analyses advisable. Pierson and Moskowitz [107] suggested a PSD for a fully developed sea state as

$$S_{\rm PM}(f) = \frac{5}{16} H_{\rm s}^2 T_{\rm p}^{-4} f^{-5} \exp\left(-1.25 \left(T_{\rm p} f\right)^{-4}\right) \tag{19}$$

following the formulation in the standard ISO 19901-1 [108]. The variable $H_{\rm s}$ is the significant wave height, a statistical measure of the height of waves in a sea state as described in [108], f is the frequency in cycles per second, and $T_{\rm p}$ is the peak period of the spectrum.

Based on data collected in the Joint North Sea Wave Observation Project (JONSWAP) [109], it was concluded that the wave spectrum is never fully developed due to nonlinear wave–wave interactions. A modification to the Pierson–Moskowitz PSD was suggested as

$$S_{I}(f) = \alpha(r) S_{PM}(f) r^{q}$$
(20)

The definitions of $\alpha(r)$, q, and r can be found in [108]. Examples of frequency functions for the JONSWAP PSD are shown in Fig. 7. A realization of a time series is shown in Fig. 7(b), with a marginal distribution of the realizations illustrating that the underlying stochastic process can be assumed to be Gaussian.

The significant wave height $(H_{\rm s})$ and peak period $(T_{\rm p})$ are fitted to site specific data. A 3-parameter Weibull distribution is suggested for $H_{\rm s}$ [110] and a lognormal distribution for $T_{\rm p}$ [111]. The calculation of stress ranges from wave heights requires structural models, typically finite element models (FE models), for spectral or time domain analyses [99].

3.1.3. Wind loading

Wind load is characterized by the mean wind speed and turbulence. The latter is decisive for fatigue deterioration while changes in mean wind speed vary slowly, resulting in few load cycles over the service life. The turbulence is, however, dependent on the mean wind speed. The probability distribution of mean wind speeds over an extended period of time is typically assumed Weibull distributed as [112]

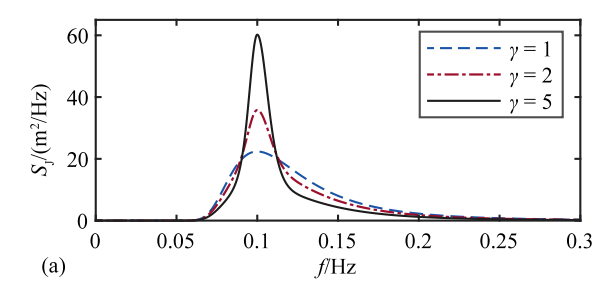
$$P(V_0) = 1 - \exp\left[-\left(\frac{V_0}{C_v}\right)^k\right] \tag{21}$$

where V_0 is the mean wind speed for a reference period of 10 min, C_v is the scale parameter of the Weibull function, and k is the shape parameter. The distribution function expresses the probability that the mean wind speed is lower than V_0 . The fraction of time that the wind speed acts within a specified interval can be calculated as $P\left(V_2\right) - P\left(V_1\right)$. It is recommended that C_v and k are determined from real data for the site. In lack of data, recommended values for the annual average value of the wind speed, $V_{\rm ave}$, and the shape parameter can be used to estimate C_v as

$$C_v = \frac{V_{\text{ave}}}{\Gamma(1+1/k)} \tag{22}$$

where $\Gamma(\cdot)$ is the Gamma function.

With an occurrence of a wind speed (interval) estimated by Eq. (21), its associated turbulence can be modelled by a PSD. The established



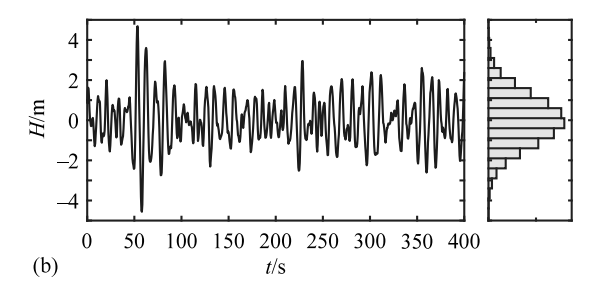
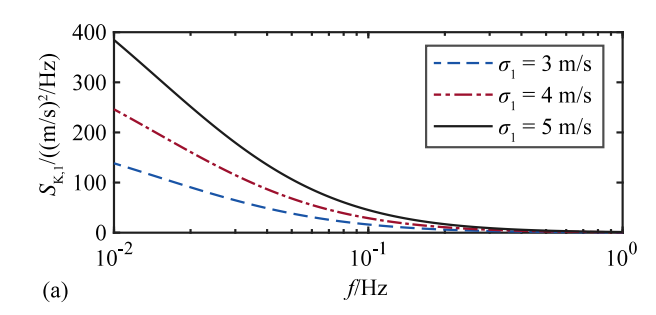


Fig. 7. PSDs for the JONSWAP model (a) and a simulated time series for $\gamma = 5$ (b). The significant wave height is set to $H_s = 5 \,\mathrm{m}$ and the peak period to $T_p = 10 \,\mathrm{s}$.



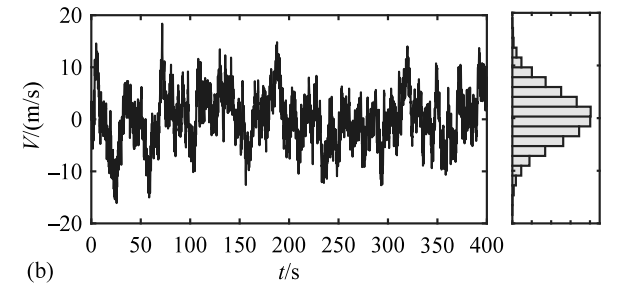


Fig. 8. PSDs for the Kaimal model (a) and a simulated time series for $\sigma_1 = 5 \, \text{m/s}$ (b). The scale parameter is set to $L_1 = 170 \, \text{m}$ and the mean wind speed to $V_z = 25 \, \text{m/s}$.

choice is the Kaimal PSD based on extensive measurements from Kansas in the Midwestern United States [113]. Following the notation in the standard IEC 61400-1 [112] the frequency function can be calculated as

$$S_{K,j}(f) = \frac{\sigma_j^2}{f} \frac{4fL_j/V_z}{(1 + 6fL_j/V_z)^{5/3}}$$
 (23)

where $j=1\dots 3$ is an index representing the longitudinal, lateral, and upward velocity components, respectively; σ_j is the turbulence standard deviation for direction j, L_j is an integral scale parameter, and V_z is the 10 min mean wind speed at the height z, which for wind turbines is set to the height of the centre of the wind turbine rotor above the terrain surface (denominated hub height). Examples of frequency functions for the Kaimal PSD are shown in Fig. 8.

A Weibull distribution is suggested for the turbulence σ_k in Eq. (23) conditional on the wind speed and shape coefficient dependent on I_{ref} , being a reference value for the turbulence intensity. More details about the parameters can be found in [112].

Dynamic simulations using structural models (e.g., FE models) are needed to retrieve stress ranges from operational modes, wind speeds, and turbulence. In addition, for wind turbines, the stress ranges obtained from simulated time series are highly dependent on the wind turbine's control system and the blade aerodynamics. Time intervals with fault conditions as well as wake effects may contribute significantly to the accumulated fatigue. It should be noted that the number of stress cycles is large for wind turbines, implying the need to consider the complete spectrum distribution. Similar fatigue load models but without the control system can be applied for other structural systems such as buildings and chimneys.

3.2. Traffic loads on bridges

Traffic loads consist of vehicles with characteristics such as axle loads, spacing of axles, and speed. The load effect from a specific vehicle can be considered close to deterministic, meaning that the load effect can be estimated with high accuracy if the vehicle's properties are known. The randomness associated with traffic loads originates from traffic volume, the mixture of vehicles (and their actual loads), dynamic effects, and – for road bridges – the lateral positions in the lanes. The resulting stress range spectrum depends on the combination of axle load

configuration and the influence line for a specific structural detail. A probabilistic fatigue assessment should therefore build upon models for realistic vehicles. Suggestions can be found in standards such as the Eurocode part 1991-2 [114]. Still, the traffic volume and mixture of vehicles need to be assigned case specifically.

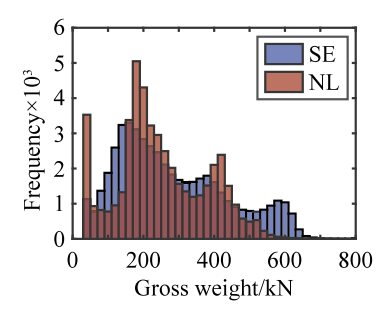
With the weigh-in-motion (WIM) technique, the characteristics of passing vehicles can be determined without disturbing the traffic [115]. It builds on sensors along the road/railway or installed on bridges (BWIM), transforming the bridge to a scale [116]. The technique enables a determination of traffic loads relevant for the considered structures, but it comes with a measurement uncertainty.

3.2.1. Loads on road bridges

The Eurocode load models for fatigue assessment (FLM1 to FLM4) were derived and calibrated against WIM measurements performed in 1986 in Auxerre, France [117,118]. Fatigue load model 4 (FLM4) is a set of standard lorries derived to give load effects equivalent to typical traffic on European roads [114], and it is more suited for probabilistic assessment than the other models. Load models from the American AASHTO specifications are described in [119], together with a model development approach using WIM data.

An example of more recent WIM data is from measurements performed 2018 along the motorway A16 near Moerdijk in the Netherlands [120]. It consists of about 240 000 heavy vehicles (\geq 35 kN). The vehicle gross weights and number of axles are presented in Fig. 9. In the same figure, data collected in Sweden from BWIM measurements between the years 2005 to 2009 are shown. It comprise about 870 000 vehicles used for fatigue calculations in [121]. There are some obvious differences in the distributions with higher gross weights in the Swedish data and more vehicles with higher number of axles. There is a clear dominance of five axle vehicles in the data from the Netherlands. This can be explained by legislation on maximum allowed gross weights for regular traffic, prescribed to 50 metric tonnes in the Netherlands (excluding exemption permits) and 60 tonnes in Sweden at the time of the measurements.

As exemplified by Fig. 9, significant regional differences exist which needs to be considered in the modelling of traffic loads. Additional examples where WIM data have been used for fatigue assessments can be found in [122–126].



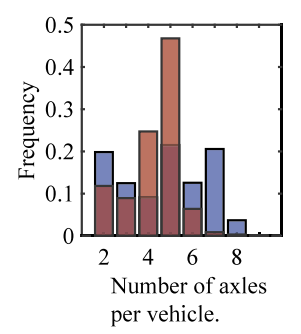


Fig. 9. Data for road vehicles from WIM measurements in the Netherlands (NL) and Sweden (SE) reproduced after [120,121], respectively.

The analysis routines for WIM measurements are typically calibrated to give static values for axles loads and gross weights. Hence, the dynamic effects caused by road surface roughness, expansion joints, the dynamic properties of the structure, and the vehicle–structure interaction need to be considered explicitly. A multiplicative stochastic variable for dynamic amplification is suggested for extreme load effects by [127] as normal distributed, with a mean value of 1.1 and a standard deviation of 0.1. It may be conservative for heavy vehicles based on measurements in [128]. Moreover, the dynamic amplification consists of bias and scatter. Hence, for the fatigue limit state it is usually conservative to use a single multiplicative value for each stress range. To date, it remains a challenge to estimate or predict a distribution for fatigue-relevant dynamic amplification.

3.2.2. Loads on railway bridges

The load carrying capacity of a railway line is classified by vehicle models with specified characteristics. In Europe these are defined by the standard EN 15528 [129]. The vehicle models are built up by wagons with axle loads in the range of 10 tonnes to 25 tonnes, and realistic axle configurations possible to implement in a fatigue assessment. Regional amendments are necessary if other trains are allowed. Imam et at. [130] combined models representative for historic trains with today's governing models for a probabilistic fatigue assessment. The annual vehicle frequency, a stress uncertainty factor, and dynamic amplification were modelled as stochastic variables on the load side.

As for road bridges, WIM and BWIM measurements can be used for registering vehicle loads with sensors mounted on the track or on bridges. North American load models for fatigue analyses based on measurements have been suggested by [131], and updated with more measurements by [132]. For specific vehicle types, the scatter in gross weights and axle loads are small with CoVs around 4%.

Dynamic effects in railway bridges are caused by the transient response of the train entering and leaving the bridge, repetitive loading of axles and bogies, vehicle–structure interaction, and rail irregularities. Amplification factors to consider these phenomena are reviewed in [133]. For code based assessments, the Eurocode EN 1991-2 (Annex D) [114] suggest an additive dynamic enhancement of

$$\varphi = 1/2 \left(\varphi' + 1/2 \varphi'' \right) \tag{24}$$

where φ' is associated to the dynamic behaviour of the structure with a perfect track, and φ'' is associated to vertical rail irregularities. Both factors are defined in [114]. The load effect should be multiplied with a factor $(1+\varphi)$. The statistical background for Eq. (24) is not documented which makes the model in the code difficult to associate with a stochastic representation.

An alternative model for dynamic amplification is presented in [134] based on data from [135]. About 1800 train passages were registered for 37 different steel beam bridges. Lognormal distributions were shown to give the best fit with parameters dependent on train speed, span length and whether the track had ballast. Mean values of the amplification factor were found to be between 4% to 22% and CoVs in the range 3% to 12% depending on the conditions.

3.3. Model uncertainties

The calculation of load effect from acting loads requires structural analyses that involve modelling choices by the analyst. The output is associated with uncertainties that need to be considered in a probabilistic assessment. Suggestions for model uncertainties associated to the loads are listed in Table 2. The structural analyses of wind and wave loaded structures need to include dynamic behaviour. Therefore, an associated uncertainty factor is listed in the table. For bridges, the structural response is typically calculated using quasi-static analyses adding a dynamic amplification to the response as a separate stochastic variable.

The model uncertainties listed in Table 2 need to be aligned with the detailing of the analyses. Other relevant factors for wind and wave loaded structures can be found in [137,138]. For bridges, model uncertainties are discussed in [136].

For existing structures, in-service monitoring provides a possibility to significantly reduce the uncertainties related to the loads and load effect estimation. Strain measurements can be used to directly determine the stress history at critical locations [54]. The model uncertainties in Table 2 including dynamic increments should then be replaced by a stochastic variable for measurement errors. A lognormal distribution is suggested with a mean value of one and a CoV in the range 2% to 5% [16,98].

4. Fatigue and structural reliability

The reliability of structural details is generally defined as

$$R(t) = 1 - \Pr\left[\min_{\tau} g(\mathbf{X}, \tau) \le 0 \quad \text{for all } 0 \le \tau < t\right]$$
 (25)

wherein $g(\mathbf{X},t)$ is the limit state function describing failure and Pr denotes probability. This definition reflects that failure in deteriorating systems is a first-passage event [25]. This is relevant when modelling fatigue failure with the LSF of Eq. (15) reflecting brittle failure.

When using the simpler LSF of Eq. (12) or when modelling fatigue with the S-N model, $g(\mathbf{X},t)$ is non-decreasing with increasing t. In these cases, Eq. (25) reduces to:

$$R(t) = 1 - \Pr[g(\mathbf{X}, t) \le 0]$$
 (26)

This point-in-time formulation is easier to evaluate than the first-passage probability of Eq. (25) [142].

The reliability is often expressed through the reliability index β defined as:

$$\beta(t) = \boldsymbol{\Phi}^{-1} \left[R(t) \right] \tag{27}$$

where Φ^{-1} is the inverse of the cumulative function of the standard normal distribution.

The reliability is straightforward to evaluate with standard reliability methods if models of the random variables **X** are available (e.g., [23]). One of the most common reliability methods is FORM (first order reliability method), originally proposed by Rackwitz and Fiessler [143]. When modelling the load as a stochastic process, computations are more challenging (e.g., [88,144]). Such an approach is relevant when load sequence effects and crack retardation and acceleration need to be considered, but it is not commonly applied in reliability analyses because of modelling and computational challenges.

Ultimately, fatigue failures of structural details are only relevant if they lead to consequences. Such failures may or may not result in global collapse of a structure. This mainly depends on the possibility to redistribute forces from a fatigue weakened part to other parts of the structure and on the material toughness. As an example, major fatigue cracks were detected in the Hoan bridge (preceded by a loss of equilibrium of one joint), which caused large deformations but did not lead to overall collapse [145]. In contrast, a suspension span of the I-95 Mianus river bridge collapsed completely because of a fatigue crack (preceded by corrosion damage of another component) [146].

Table 2Examples of model uncertainties associated to load modelling in structural analyses for fatigue assessment given as load or stress multiplication factors.

Description	Distribution	Mean	CoV	Source
Nominal stress calculation	Lognormal	1	0.10	[25,136]
Stress concentration calculation	Lognormal	1	0.20	[25]
	Normal	1	0.05	[43]
Wind and wave loads	Lognormal	1	0.10 to 0.20	[137-139]
Dynamic response (wind and wave)	Lognormal	1	0.05	[137]
Traffic load models	Normal	a	0.10 to 0.20	[140]
WIM measurement uncertainty	System-depend	ent		[141]

^a Load-model dependent.

Hence, even though fatigue limit states (FLS) can in some cases directly lead to collapse, they are treated differently than other ultimate limit states (ULS). The three main reasons for this difference are:

- i. Fatigue cracks can be detected in time by dedicated inspections or the users of a structure, provided the material is sufficiently tough. However, in case of low toughness, fatigue failure is characterized by a lack of plastic redistribution and a lack of warning.
- ii. Fatigue is about details (such as connections) rather than components. A structure can contain a large number of details. A system reliability analysis can be applied to evaluate the reliability of the entire structure conditional on the fatigue failure(s) of the detail(s).
- iii. Whereas other limit states are usually reached at extreme loads, at which often multiple components fail simultaneously, the fatigue limit state can be reached at quite ordinary load levels at different points in time.

As a result of the latter two aspects, combined with the large scatter in fatigue resistance, the dependence among fatigue failure events at different details is lower than for other ULS [147].

In offshore engineering, the relation between fatigue failures and ultimate collapse is quantified by the change in reserve strength or the probability of collapse when fatigue failures occur [148,149]. This is then used to derive acceptable reliability levels for fatigue failures. However, these models neglect that fatigue failures are dependent, i.e., that they are likely to occur in clusters. This dependence can strongly affect the structural system reliability for given levels of fatigue reliability. A system reliability models to account for this were proposed in [147,150].

Repair of detected cracks is often made dependent on estimates of the probability of global collapse. In some cases, crack growth is closely monitored until a convenient time for repair or replacement. However, such a strategy has been demonstrated to be dangerous in some cases, as cracks can grow in unexpected directions and 'jump' to other parts of a structure, e.g., observed in some of the collected cases in [151].

The differences between FLS and ULS can lead to requiring different target reliability levels. The choice of the target reliability level must consider both safety and economic risks to society, with typical maximum acceptable probabilities of failures in the order of 10⁻⁶ to 10⁻⁵ per year for ULS [25]. The initial values for target reliability recommended for fatigue are given in the Eurocode background document [152]. These values came from the Eurocode 3 draft. They are similar to a proposal made by the Transportation Research Board Program in the USA, which investigated the fatigue safety of road bridges [153]. There, a distinction is made between design details in statically indeterminate load-bearing elements versus statically determinate ones. For the former, a reliability of 97.7%, or a reliability index $\beta = 2$ referring to the entire design life, is considered as safe while for the latter a reliability of 99.87%, corresponding to $\beta = 3$, is required. Since then, based in particular on the work of the JCSS, all have converged towards higher values that are similar in most structure standards, but depending on the type of structure; the target reliability levels for structures such as bridges [154] are higher than those for

wind turbine towers [112]. For fatigue of structures not designed for inspection and/or difficult to repair, the target reliability levels in most structural standards are the same as for other ULS states.

Examples where inspections are implicitly considered to accept lower reliability levels than those for ULS – namely, $\beta = 2$ –3 for the entire life – are documented in [121,153]. Such an approach is not opposed by the standards, but it should be taken critically; the added value of the inspection is a function of the type and frequency of inspections. In such a case, it is advocated to use a FM assessment in which the inspections are explicitly considered (see Sections 5.2 and 6.2), so that target reliability levels equal or similar to other ULS apply.

The failure probability for fatigue follows a "bath tub" curve [155], with a relatively high failure rate at short lives (due to the probability of low quality details, e.g., with large misalignment or undercut in welded details) as well as at long lives (due to the progressive nature of fatigue) and a lower failure rate in between. One needs to use FM to model this behaviour. Ignoring this, and using Eq. (7), the highest failure probability occurs in the last period of the design life. Given this nature, one could debate if a target reliability defined for the entire design life is the best choice; a target for a shorter reference period like an annual target reliability level may be more appropriate. It should be noted that the 50 years and 1 year target reliability levels in EN 1990 [154] are consistent only if all random variables are independent in time, which is not the case for fatigue limit states.

5. Semi-probabilistic treatment of fatigue in standards

5.1. Historical development

The safety factor principle is as old as the use of design calculations in engineering practice. For most times, the use of a global safety factor was common. Pioneering work on the modern partial safety factor principle started in the 1950s in Denmark [24]. Following advanced machinery designs and research in the same period, which led to increased extreme loads on components (including fatigue), a major research effort was made in structural engineering through the 1960s and 1970s. These led to substantial changes to the provisions in the design specifications for steel structures and to the first fatigue design rules. The first standards that considered fatigue were the German standard [156], the British standard [157], part 10, and the 1974 AASHTO fatigue specifications [158].

On the resistance side, these standards contained different detail categories. The mean stress influence was accounted for through a Smith diagram (German standards) and/or different S-N curve slope coefficients. It was disregarded for welded details in the British standards and AASHTO specifications by conservatively defining S-N curves corresponding to high mean stress, R=0.5, as initially recommended by [159]. This was followed by the first European ECCS recommendations in 1985 [160], which contained unified rules with a standardized set of parallel S-N curves, still in use today in the Eurocodes. For defining design S-N curves, the 95% confidence limits (97.5% survival limits) were used, accounting for the size of the dataset used to estimate the aleatory and epistemic uncertainties. In EN 1993-1-9 a 95% probability of survival with a 75% confidence level is used

for the determination of the S-N curve constant $\log(K1)$, see [161] for details. In today's draft of EN1990 and as presented in Section 2, this has slightly changed, since the above interval is not consistent with Annex D of EN 1990. Now a prediction interval using Baysian statistics to get a 95% probability of survival is used instead. Based on the work of the JCSS, the ECCS recommendations also contained the first comprehensive description of partial safety factors determination based on semi-probabilistic treatment of fatigue to meet a target reliability (so-called level II method).

The theory of structural reliability offers several methods to find partial factors corresponding to the target reliability β_t level. The ECCS recommendations [160] and Eurocode background document 9.01 dated 1989, re-edited [152], developed explicit expressions for a linear limit state function expressed with the S-N curves and global load S and resistance R variables being lognormally distributed. Run-out test results were not included, but the number of cycles associated with the CAFL is loosely based on run-out data. The characteristic fatigue loads are then multiplied by partial factor γ_S and the fatigue resistances divided by a partial factor γ_R , or a combined safety factor $\gamma = (\gamma_S * \gamma_R)$ is adopted. As an example, using the FORM design point, the fatigue partial resistance factor can be expressed in function of the relevant variables as follows:

In case of relatively high stress ranges (1st stage of the S-N curve is relevant):

$$\log_{10}(\gamma_R) \approx \left(\alpha_R \beta - k\right) \frac{\sigma_{log} K_1}{m_1} \tag{28}$$

In case of relatively low stress ranges (2nd stage of the S-N curve is relevant):

$$\log_{10}(\gamma_R) \approx \frac{\alpha_R \beta \sqrt{\sigma_{logK2}^2 + [\log_{10}(\exp(V_{Dlim}))]^2} - k \cdot \sigma_{logK2} - \log_{10}(\mu_{Dlim})}{m_2}$$
(29)

where V_{Dlim} is the CoV of D_{lim} , α_R is the FORM sensitivity factor for the fatigue resistance and k=1.65 or k=2 for the characteristic S-N curve defined as the 95% or 97.5% survival fractile, respectively. Using the distribution parameters of Table 1, the two equations give approximately the same partial resistance factor. The above is for illustration purpose only, as it is based on assumptions such as small coefficients of variation. Nonetheless it shows the importance of the influence of the definition of the characteristic resistance (via k), S-N curve slopes, and variability of the damage at failure on the resistance factor.

Since the 1990s, the basis of the safety requirements remained, but many investigations and further developments were made, in particular due to the exponential increase in computing power. These have led to modifications in the limit state functions to better model reality, including more variables and correlations, load cases, inspection results, etc. Furthermore, reliability differentiation has been investigated, considering annual versus life time reliability targets, as well as minimum versus average life-time reliability. For fatigue, this is an ongoing task, it will certainly not be finished with the publication of the second generation of Eurocodes (in 2024–2026). An example of such a recalibration for the design of steel road bridges can be found in [136].

5.2. Safety factors related to consequences of failure and inspectability

Fatigue standards contain different concepts to deal with fatigue reliability, which can be summarized as follows [162]:

- Infinite life design, based on keeping actions under an assumed fatigue strength limit.
- Safe life design, based on ensuring that no fatigue cracks will form, i.e., no detectable cracks during the whole service life. If any cracks appear, they are at the initiation stage.

- Fail safe design, in which the structure is designed to tolerate extensive fatigue cracking without failing, possibly because the structure is statically indeterminate or adequately redundant.
- Damage tolerant design, which allows fatigue cracks to form but ensures that they are readily detectable in service before becoming critical.

The first three concepts can be evaluated using the limit state functions in Section 2. In a fail safe design, lower reliability indexes for the individual fatigue limits states can be acceptable due to the lower consequence of failure of individual details. Damage tolerant designs can be evaluated with an FM approach, where the probability distributions of the model parameters are updated with the inspection results using Bayesian analysis, as outlined in Section 6.2.

Note that the above four concepts can be combined, in particular, one often chooses to combine a damage tolerant design together with a fail-safe design in order to have sufficient opportunities to detect and repair cracks that have developed. In the standard EN 1993-1-9 [41] and now prEN 1993-1-9 [163], the concepts 2 and 4 are explicit but in fact all of the four are inherent, often combined. In case of safe life concept, one must ensure an acceptable reliability for the structure's design life without the need for regular inspection nor maintenance. Thus, the initially high reliability index level is decreasing with time to reach the minimum (target) value at the end of the design service life, as shown in Fig. 10. In case of the damage tolerant concept, the acceptable reliability is ensured by implementing inspection and maintenance measures throughout the life of the structure. In this case, the reliability level - initially lower than that of the safe life method - reaches the minimum target value at the end of the design service life, but with periodical readjustments according to inspection results and possible resulting interventions (repairs), as quantified by Bayesian analysis following Section 6.2. The evolution of the reliability index as a function of the choice of the verification method (design concept) and the consequences of failure are reflected in the resistance factor values. Note that target reliability corresponds to the combined safety factor $\gamma = \gamma_S * \gamma_R$, thus requiring the load model to be defined simultaneously.

6. Life-cycle management of structures subject to fatigue

6.1. Maintenance strategies

Engineering structures must comply with reliability targets over their service life following Section 4. For structures subject to fatigue, these reliability targets may be reached by any of the concepts listed in Section 5.2. However, given the large uncertainties associated with fatigue deterioration, the infinite life and safe life design approaches lead to a substantial safety margin, which can be uneconomical or even infeasible. Also, for existing structures, these approaches are often not possible due to the difficulties associated with modifying existing structural details. This can motivate the use of the damage tolerant concept, which require an adequate maintenance strategy.

One distinguishes between corrective and preventive maintenance strategies [164]. In a corrective strategy, components are replaced upon failure. Such a strategy is only possible when individual fatigue failures are not critical for the structural integrity, such as in a fail safe design. Additionally, it must be ensured that fatigue failures are detected and repaired. For most civil engineering and offshore structures, these conditions are not fulfilled and a preventive maintenance strategy is necessary.

Preventive maintenance is based on identifying deteriorating elements prior to their failure and performing appropriate maintenance actions. For fatigue, inspection is the common means to identify these elements, although the use of monitoring is increasingly considered (e.g., [165]). Inspections can be visual or by means of non-destructive evaluation (NDE). For certain types of structures, minimum inspection



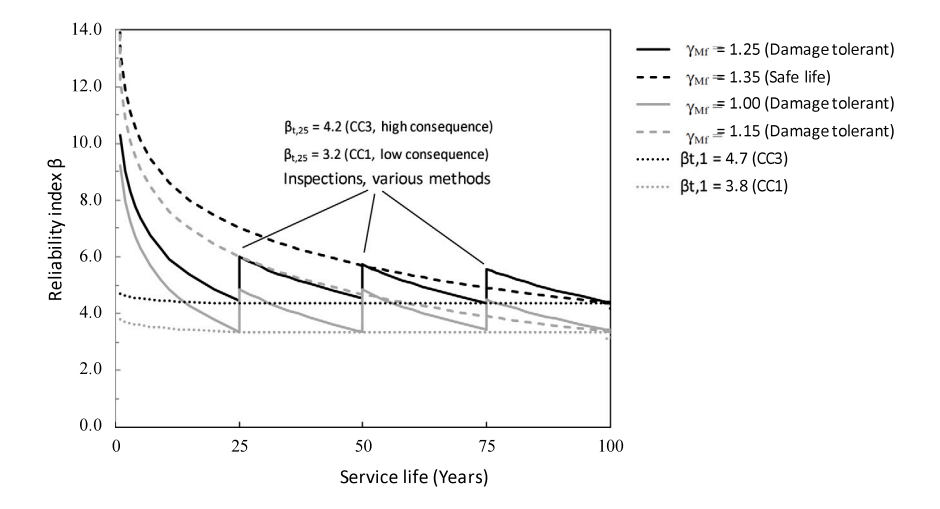


Fig. 10. Evolution of the reliability index with time, influence of concept and inspections. The consequence class (CC) refers to the concept in EN 1990 [154].

intervals are prescribed and implemented, e.g., for bridges [166]. As pointed out in Section 5.2, inspections are considered in codes as a means to ensure the safety of structures. However, the extent and frequency of these inspection is typically not specified. Reliability and risk-based inspection planning has been developed to specify the necessary or optimal inspection efforts. These methods are based on the updating of the fatigue reliability with inspection results. The following sections give an overview of these methods.

6.2. Bayesian updating of fatigue reliability

Inspections reduce uncertainty, which can be quantified through updating the probabilistic models or directly the reliability by means of Bayes' rule [167–169]. Thereby, the a-priori probability of failure $\Pr(F)$ is updated to the posterior probability of failure given the inspection outcome Z. In fatigue reliability, the updating is traditionally performed through the definition of the conditional probability as [168]

$$Pr(F|Z) = \frac{Pr(Z \cap F)}{Pr(Z)}$$
(30)

While the failure event F is modelled through the limit states, as in classical fatigue reliability analysis (cf. Section 4), the observation event Z is modelled by means of the likelihood Pr(Z|X). The likelihood describes the probability of inspection outcomes given the basic random variables X or any function thereof, such as the crack size. In the case that the observation is the detection or no-detection of a crack, the likelihood is the Probability of Detection (PoD) curve, which gives the probability of detecting a crack at the inspection in function of the crack size a [170]. Such PoD models are available from the literature [43], inferred from tests [171,172], from in-service inspections [173] or from simulations. An example of a PoD curve is shown in Fig. 11. For depth inspection techniques, e.g. based on ultrasonic waves, the PoD is best expressed in terms of crack depth. For surface inspection techniques based on magnetic particles or dye penetrant, the PoD curve is best expressed in terms of the semi surface length c, although it is possible. as in Fig. 11, to express it in terms of crack depth if that is the decisive parameter for the fatigue reliability.

As an example, Fig. 12 shows the reliability of a fatigue detail updated with the information that no crack was found at inspections.

Amongst different options, Markov chains have been frequently applied to facilitate Bayesian updating in estimating the probability of a state change (e.g., from a measured to a critical crack size, [176,177]). The advantage of this alternative is its easy and fast computation, its disadvantage is that it does not properly model (time-invariant) model uncertainties, which are not Markovian.

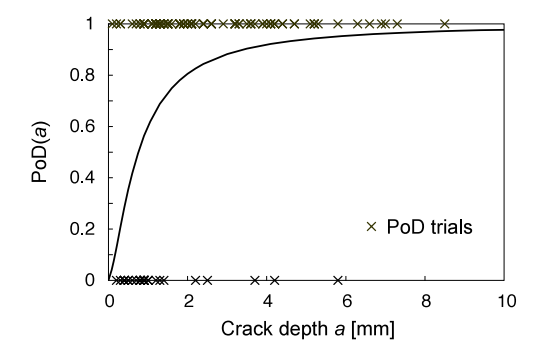


Fig. 11. Probability of Detection (PoD) curve for magnetic particle inspections of welded connection in tubular joints of offshore structures. The PoD curve is learned from the indicated data that was collected in the ICON project [174]. *Source:* Figure reproduced from [175].

6.3. Reliability-based inspection planning

To optimize inspection within the preventive maintenance approach, reliability and risk-based inspection planning has been developed for structures subject to fatigue, mainly in the offshore domain following the collapse of the "Alexander L. Kielland" platform, although first approaches were reported for aircraft structures already in the 1970s [178]. These approaches are based on explicitly evaluating the fatigue reliability and updating it with inspection outcomes using Bayesian methods. They mostly work at the level of structural details.

In reliability-based inspection planning, inspection times are set to ensure a minimum level of reliability throughout the lifetime of the structure. Based on a model of the reliability of fatigue details over time (including inspections following Section 6.2), the inspection time is determined to ensure that the acceptable reliability level is not crossed.

Inspection plans have been considered by assuming that either any inspection results in a no-detection event \bar{D} or an identified fatigue crack is managed, e.g., by an immediate repair [13,14]. Traditionally, two types of inspection plans were considered: the equi-distant plan and the threshold plan [179]. In the equi-distant plan, inspections are planned at fixed time intervals. One then chooses the longest time inspection interval that ensures compliance with the acceptable reliability level. In the threshold plan, inspection times are chosen whenever the predicted reliability is about to fall below the acceptable reliability level (the threshold). Fig. 12 illustrates the threshold plan. Inspection times are determined by ensuring that a probability of fatigue failure threshold is not exceeded. The threshold 10^{-4} yr⁻¹ leads to significantly higher number of inspections than the threshold 10^{-3} yr⁻¹.

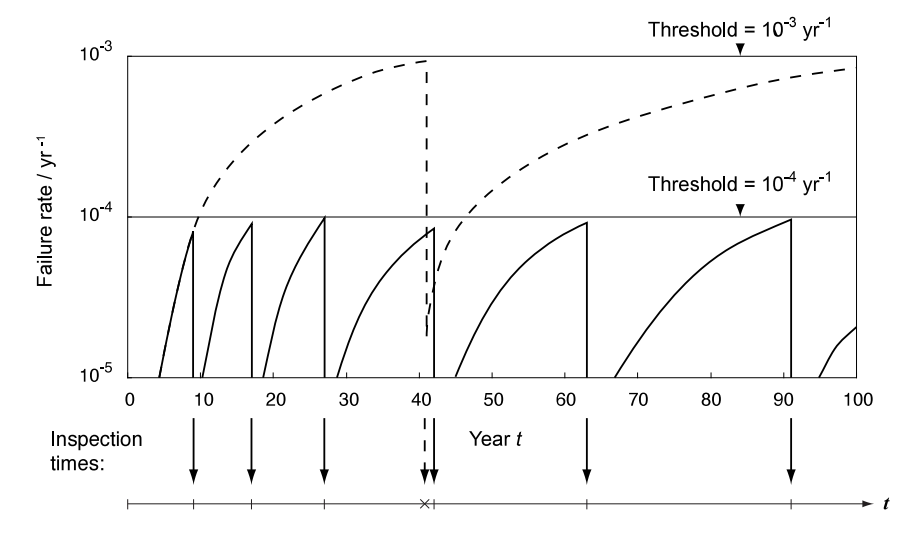


Fig. 12. Probability of fatigue failure over time for different inspection schedules. The fatigue failure probability is determined conditional on no-detection of a defect at all inspections using Bayesian updating.

Source: Adapted from [175].

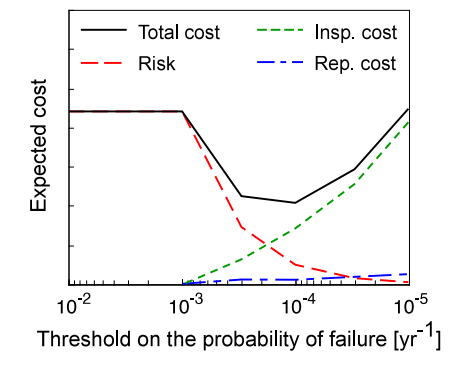


Fig. 13. Expected life-cycle cost for a fatigue detail in function of the probability of failure threshold. In risk-based inspection, the inspection plan associated with the lowest expected cost is selected, here the one corresponding to a threshold of 10⁻⁴ yr⁻¹.

To account for the relation between the reliability of the fatigue detail and the structure, the reliability threshold can be determined in function of the importance of the detail for the structure. Following Section 4, the importance can be quantified by the probability of structural collapse given a fatigue failure. The acceptable probability of failure of the fatigue detail then follows from the reliability target for the structural system [147]. Alternatively, the minimum acceptable probability of fatigue failure can be specified separately for details that belong to primary, secondary or tertiary structural members.

6.4. Risk-based inspection planning

By explicitly quantifying the consequences of failure, the risk associated with fatigue failures can be quantified as the product of the fatigue failure probability and the consequences of failure. The consequences are thereby determined in function of the importance of the structural detail for the structural integrity, following Section 4. If the consequences are quantified in monetary terms, it is possible to perform a risk-based optimization of inspection efforts.

As shown in Fig. 12, the inspection efforts determine the reliability of the fatigue detail, and hence the risks. By balancing the cost of the inspections (and the repairs following inspections) with the risk, an optimal inspection effort can be determined, as illustrated in Fig. 13.

Risk-based inspection planning is more challenging when considering an optimization at the structural system level and when considering inspection and monitoring that result in information other

than just detection/no-detection of fatigue cracks. Recent works have addressed these aspects to derive optimal inspection plans for structural systems [180-183].

Even in risk-based inspection planning it must still be ensured that the reliability targets are fulfilled. For this reason, risk-based inspection planning is seldom applied in practice for structures with potential loss of life; instead inspections are performed following reliability-based inspection plans.

7. Concluding remarks

This paper gives an overview of probabilistic fatigue load and resistance models for steel structures, as well as methods for evaluating and assessing the structural reliability. This includes the effects of inspections and maintenance strategies. While fatigue reliability assessment is commonly employed and has reached a mature state, current approaches used in practice still have significant limitations, which should be addressed in the future. Some important points are summarized in the following.

- · The fatigue resistance is obviously subject to large scatter. The scatter appears to be larger at low stress range levels. The Basquin relationship evaluated with the least squares method, as often applied in practice and used as the basis for standards, does not consider this. It also does not consider the information contained in run-outs. S-N models and parameter estimations are available that do take these aspects into account.
- · A good estimate of the distribution parameters of any S-N curve requires a relatively large test database containing different test series. There is a risk of underestimating the scatter in fatigue resistance in case of a small test database. A generally accepted procedure for establishing the fatigue resistance based on a small number of tests is currently lacking. This is a topic for future research.
- · The largest uncertainty in the fatigue resistance is in the damage created by stress ranges lower than the constant amplitude fatigue limit in a variable amplitude load spectrum.
- · Measurement campaigns have provided insights into fatigue relevant loads. The largest uncertainties on the load side arise from the (accuracy of the) engineering model and the dynamic interaction between load and structure. These are areas for future research.

- Fatigue is an ultimate limit state. However, some characteristics, such as the possibility to detect cracks before failure occurs, motivate a different treatment of fatigue limit states. For this reason, the target reliability values can differ from other ultimate limit states. A consensus is needed to obtain generally accepted values for the target reliability for fatigue. This applies to both failure of individual details as well as failure of the entire structure.
- Reliability- and risk-based inspection planning are effective ways to address the high scatter and large uncertainty of fatigue in engineering structures. More explicit considerations of the effects of inspections in fatigue codes and standards is however lacking.
- Possible (future) additions to the JCSS Probabilistic Model Code are: Alternative (more realistic) fatigue resistance models (inclusion of random fatigue limit models, description of the FAC, consideration of load sequence effects), description of probabilistic fatigue load models, and more explicit procedures for reliability- and risk-based inspection planning.

CRediT authorship contribution statement

Johan Maljaars: Conceptualization, Methodology, Writing – original draft, Writing – review & editing. John Leander: Methodology, Writing – original draft, Writing – review & editing. Alain Nussbaumer: Methodology, Writing – original draft, Writing – review & editing. John Daalsgaard Sørensen: Methodology, Writing – original draft, Writing – review & editing. Daniel Straub: Conceptualization, Methodology, Writing – original draft, Writing – review & editing.

Declaration of competing interest

The authors declare that they have no known competing financial interests or personal relationships that could have appeared to influence the work reported in this paper.

Data availability

Previously published data is used, references are given.

References

- Wöhler A. On the structural tests with iron and steel [über die festigkeitsversuche mit eisen und stahl]. Z Bauwesen 1870;40:73–106.
- [2] Joint Committee Concerning the Ashtabula Bridge Disaster. Report of the joint committee concerning the ashtabula bridge disaster under joint resolution of the general assembly. House of Representatives of the State of Ohio, for the Adjourned Session of the Sixty-Second General Assembly. Volume LXXIII. Elifritz and Winter, Springfield, Ohio; 1877.
- [3] Imam B, Chryssanthopoulos MK. Causes and consequences of metallic bridge failures. Struct Eng Int 2012;22:93–8.
- [4] Proske D. Comparison of probability of failure and collapse frequency of bridges [vergleich der versagenswahrscheinlichkeit und der versagenshäufigkeit von brücken]. Bautechnik 2017;94:419–29.
- [5] Naesheim T. The Alexander l. kielland accident: report presented to ministry of justice and police March 1981. Ministry of Justice and Police, Norway; 1981, ISBN B0000ED27N.
- [6] Mai QA, Weijtjens W, Devriendt C, Morato PG, Rigo P, Sørensen JD. Prediction of remaining fatigue life of welded joints in wind turbine support structures considering strain measurement and a joint distribution of oceanographic data. Mar Struct 2019;66:307–22.
- [7] Pelayo F, Rodríguez C, Canteli A. Failure and repair analysis of a runway beam: Influence of the standard applied to lifetime prediction. Eng Fail Anal 2015;56:89–97.
- [8] Ross B, McDonald B, Vijay Saraf S. Big blue goes down. The miller park crane accident. Eng Fail Anal 2007;14(6):942–61.
- [9] Wirsching PH. Fatigue reliability in welded joints of offshore structures. Int J Fatigue 1980;2(2):77–83.
- [10] Schilling CG, Klippstein KH. Fatigue of steel beams by simulated bridge traffic. ASCE J Struct Div 1977;103(8):1561–75.
- [11] Schilling C. Fatigue of welded steel bridge members under variable-amplitude loadings. NCHRP report 188, Highway Research Board; 1978.
- [12] Zhao Z, Haldar A. Bridge fatigue damage evaluation and updating using non-destructive inspections. Eng Fract Mech 1996;53(5):775–88.

[13] Thoft-Christensen P, Sørensen JD. Optimal strategy for inspection and repair of structural systems. Civ Eng Syst 1987;4(2):94–100.

- [14] Madsen H, Sørensen JD, Olesen R. Optimal inspection planning for fatigue damage of offshore structures. In: Proceedings of the 5th international conference on structural safety and reliability: structural safety and reliability. American Society of Civil Engineers; 1989, p. 2099–106.
- [15] Goyet J, Straub D, Faber MH. Risk-based inspection planning of offshore installations. Struct Eng Int 2002;12(3):200-8.
- [16] Kwon K, Frangopol DM. Bridge fatigue reliability assessment using probability density functions of equivalent stress range based on field monitoring data. Int J Fatigue 2010:32:1221–32.
- [17] Leander J, Andersson A, Karoumi R. Monitoring and enhanced fatigue evaluation of a steel railway bridge. Eng Struct 2010;32(3):854–63.
- [18] Liu Y, Frangopol DM. Utility and information analysis for optimum inspection of fatigue-sensitive structures. J Struct Eng 2019;145(2):04018251.
- [19] Committee on Fatigue and Fracture Reliability of the Committee on Structural Safety and Reliability of the Structural Division, American Society of Civil Engineers. Fatigue reliability: introduction. J Struct Div 1982;108(1):3–23.
- [20] Committee on Fatigue and Fracture Reliability of the Committee on Structural Safety and Reliability of the Structural Division, American Society of Civil Engineers. Fatigue reliability: Quality assurance and maintainability. J Struct Div 1982;108(1):25–46.
- [21] Committee on Fatigue and Fracture Reliability of the Committee on Structural Safety and Reliability of the Structural Division, American Society of Civil Engineers. Fatigue reliability: Variable amplitude loading. J Struct Div 1982;108(1):47–69.
- [22] Committee on Fatigue and Fracture Reliability of the Committee on Structural Safety and Reliability of the Structural Division, American Society of Civil Engineers. Fatigue reliability: Development of criteria for design. J Struct Div 1982;108(1):71–88.
- [23] Madsen HO, Krenk S, Lind NC. Methods of structural safety. Englewood Cliffs: Prentice-Hall; 1986.
- [24] Ditlevsen O, Madsen H. Structural reliability methods. New York: Wiley; 1996.
- [25] JCSS. JCSS probabilistic model code. Joint Committee on Structural Safety; 2013, URL https://www.jcss-lc.org/jcss-probabilistic-model-code/.
- [26] Ono Y, Baptista C, Kinoshita K, Yıldırım HC, Nussbaumer A. A reanalysis of fatigue test data for longitudinal welded gusset joints in as-welded and high frequency mechanical impact (HFMI)-treated state. Int J Fatigue 2021;149:106167.
- [27] Lawless JF. Statistical models and methods for lifetime data. John Wiley & Sons; 2011.
- [28] Basquin O. The exponential law of endurance tests. In: Proc am soc test mater. Vol. 10, 1910, p. 625–30.
- [29] Schijve J. Statistical distribution functions and fatigue of structures. Int J Fatigue 2005;27(9):1031–9.
- [30] Canteli AF, Castillo E, Blasón S, Correia J, de Jesus A. Generalization of the Weibull probabilistic compatible model to assess fatigue data into three domains: LCF, HCF and VHCF. Int J Fatigue 2022;159:106771.
- [31] Li H, Wen D, Lu Z, Wang Y, Deng F. Identifying the probability distribution of fatigue life using the maximum entropy principle. Entropy 2016;18(4):111.
- [32] Maddox S, Hopkin G, Holy A, et al. Improving the fatigue performance of welded stainless steels. Report EUR 22809, European Commission; 2007.
- [33] Miki C, Mori T, Sakamoto K, Kashiwagi H. Size effect on the fatigue strength of transverse fillet welded joints. J Struct Eng 1987;33A:393–402.
- [34] Gurney TR. The fatigue strength of transverse fillet welded joints: a study of the influence of joint geometry. Elsevier; 1991.
- [35] Wintergerst S, Heckel K. The fatigue strenght of plates of steel st 37 with welded transverse attachmens [die dauerfestigkeit von flachstahl aus stahl st 37 mit aufgeschweißter quersteifung]. Der Stahlbau 1966;35:353–7.
- [36] Yagi J, Machida S, Tomita Y, Matoba M, Soya I. Influencing factors on thickness effect of fatigue strength in as-welded joints for steel structure. J Soc Nav Archit Japan 1991:1991(169):289–99.
- [37] Bartsch H, Citarelli S, Feldmann M. Investigations on the fatigue behaviour of welded-in stiffeners with gaps. J Constr Steel Res 2022;189:107075.
- [38] Gurney T. Cumulative damage of welded joints. Woodhead Publishing Limited; 2006.
- [39] BS7608:2014. Guide to fatigue design and assessment of steel products. BSI; 2014.
- [40] Keating PB, Fisher JW. Evaluation of fatigue tests and design criteria on welded details. Report 286. National Cooperative Highway Research Program: 1986.
- [41] EN 1993-1-9:2005. Eurocode 3: design of steel structures part 1-9: fatigue. CEN; 2005.
- [42] Bartsch H, Drebenstedt K, Seyfried B, Feldmann M, Kuhlmann U, Ummenhofer T. Analysis of fatigue test data to reassess EN 1993-1-9 detail categories. Steel Constr 2020;13(4):280–93.
- [43] DNV-RP-C210:2019. Probabilistic methods for planning of inspection for fatigue cracks in offshore structures. DNV; 2019.
- [44] Maljaars J, Euler M. Fatigue SN curves of bolts and bolted connections for application in civil engineering structures. Int J Fatigue 2021;151:106355.

[45] Pyttel B, Schwerdt D, Berger C. Very high cycle fatigue—Is there a fatigue limit? Int J Fatigue 2011;33(1):49–58.

- [46] Sonsino CM. Course of SN-curves especially in the high-cycle fatigue regime with regard to component design and safety. Int J Fatigue 2007;29(12):2246-58
- [47] Pascual FG, Meeker WQ. Estimating fatigue curves with the random fatigue-limit model. Technometrics 1999:41(4):277–89.
- [48] Castillo E, Fernández-Canteli A. A unified statistical methodology for modeling fatigue damage. Springer Science & Business Media; 2009.
- [49] D'Angelo L, Nussbaumer A. Estimation of fatigue SN curves of welded joints using advanced probabilistic approach. Int J Fatigue 2017;97:98–113.
- [50] Leonetti D, Maljaars J, Snijder HB. Fitting fatigue test data with a novel SN curve using frequentist and Bayesian inference. Int J Fatigue 2017;105:128–43.
- [51] Akaike H. A new look at the statistical model identification. IEEE Trans Automat Control 1974;19(6):716–23.
- [52] Haibach E. The allowable stresses under variable amplitude loading. In: Gurney T, editor. Proceeding conf. fatigue welded struct.. Cambridge: The Welding Institute; 1970, p. 328–39.
- [53] Haibach E. Fatigue strength [betriebsfestigkeit]. Springer; 2006.
- [54] Kühn B, Lukic M, Nussbaumer A, Günther H-P, Helmerich R, Herion S, Kolstein MH, Walbridge S, Androic B, Dijkstra O, et al. Assessment of existing steel structures: Recommendations for estimation of remaining fatigue life. Joint Research Center; 2008, URL https://eurocodes.jrc.ec.europa.eu/sites/default/ files/2021-12/EUR23252EN.pdf.
- [55] Sørensen JD, Munch-Andersen J, Hansen SO, Sørensen FO, Christensen HH, Lind P, Poulsen A. Background studies in connection with preparation of National Annexes to EN1990 and EN1991: Safety format, load combinations, partial coefficients, fatigue, snow load, wind load [Baggrundsundersøgelser ifm. udarbejdelse af Nationale Annekser til EN1990 og EN1991: Sikkerhedsformat, lastkombinationer, partialkoefficienter, udmattelse, snelast, vindlast] DS/INF 172. Dansk Standard; 2009.
- [56] Palmgren A. Fatigue life of ball bearings [die die levbensdauer von kugellagern]. VDI-Z 1924;68:339–41.
- [57] Miner MA. Cumulative damage in fatigue. J Appl Mech 1945;12:159-64.
- [58] Wirsching PH. Fatigue reliability for offshore structures. J Struct Eng 1984;110(10):2340–56.
- [59] Kunz P, Kulak G. Fatigue safety of existing steel bridge. In: Extending lifesp. struct. san fr. IABSE symp. 1995, p. 1073–8.
- [60] Baptista C, Reis A, Nussbaumer A. Probabilistic SN curves for constant and variable amplitude. Int J Fatigue 2017;101:312–27.
- [61] Leonetti D, Maljaars J, Snijder H. Probabilistic fatigue resistance model for steel welded details under variable amplitude loading–Inference and uncertainty estimation. Int J Fatigue 2020;135:105515.
- [62] Alderliesten R. How proper similitude can improve our understanding of crack closure and plasticity in fatigue. Int J Fatigue 2016;82:263–73.
- [63] Raju I, Newman Jr J. Stress-intensity factors for a wide range of semi-elliptical surface cracks in finite-thickness plates. Eng Fract Mech 1979;11(4):817–29.
- [64] BS 7910:2019. Guide to methods for assessing the acceptability of flaws in metallic structures. BSI; 2019.
- [65] Forman RG, Mettu SR. Behavior of surface and corner cracks subjected to tensile and bending loads in a Ti–6Al–4V alloy. In: Ernst H, Saxena A, McDowell D, editors. Fracture mechanics: twenty-second symposium, ASTM STP 1131, vol. I. ASTM; 1992, p. 519–46.
- [66] Gurney TR. An analysis of some fatigue crack propagation data for steels subjected to pulsating tension loading. Weld Res Int 1979;9.
- [67] Beck A, Santana Gomes W. Stochastic fracture mechanics using polynomial chaos. Probab Eng Mech 2013;34:26–39.
- [68] Kitagawa H. Applicability of fracture mechanics to very small cracks or the cracks in the early stage. In: Proc. of 2nd ICM, Cleveland. 1976, p. 627–31.
- [69] Zerbst U, Madia M. Fracture mechanics based assessment of the fatigue strength: approach for the determination of the initial crack size. Fatigue Fract Eng Mater Struct 2015;38(9):1066–75.
- [70] Murakami Y, Endo M. Effects of defects, inclusions and inhomogeneities on fatigue strength. Int J Fatigue 1994;16(3):163–82.
- [71] El Haddad M, Topper T, Smith K. Prediction of non propagating cracks. Eng Fract Mech 1979;11(3):573–84.
- [72] McEvily A, Endo M, Murakami Y. On the relationship and the short fatigue
- crack threshold. Fatigue Fract Eng Mater Struct 2003;26(3):269–78.
 [73] Chapetti MD. Fatigue propagation threshold of short cracks under constant
- [74] Maierhofer J, Pippan R, Gänser H-P. Modified NASGRO equation for physically short cracks. Int J Fatigue 2014;59:200–7.

amplitude loading. Int J Fatigue 2003;25(12):1319-26.

- [75] Leonetti D, Maljaars J, Snijder H. Fracture mechanics based fatigue life prediction for a weld toe crack under constant and variable amplitude random block loading—Modeling and uncertainty estimation. Eng Fract Mech 2021;242:107487.
- [76] Schork B, Kucharczyk P, Madia M, Zerbst U, Hensel J, Bernhard J, Tchuindjang D, Kaffenberger M, Oechsner M. The effect of the local and global weld geometry as well as material defects on crack initiation and fatigue strength. Eng Fract Mech 2018;198:103–22.

[77] Kountouris I, Baker M. Defect assessment. Analysis of defects detected by MPI in an offshore structure. CESLIC report no. OR6, London, U.K.: Imperial College; 1080

- [78] Engesvik KM, Moan T. Probabilistic analysis of the uncertainty in the fatigue capacity of welded joints. Eng Fract Mech 1983;18(4):743-62.
- [79] Shetty N, Bakler M. Fatigue reliability of tubular joints in offshore structures-reliability analysis. In: Proc 9th OMAE. 1990, p. 231–340.
- [80] Zhao W, Stacey A. Review of defect distributions for probabilistic structural integrity assessment. In: International conference on offshore mechanics and arctic engineering, Vol. 36134, 2002, p. 607–19.
- [81] Huther I, Primot L, Lieurade H, Janosch J, Colchen D, Debiez S. Weld quality and the cyclic fatigue strength of steel welded joints. Weld World 1995;2(35):151.
- [82] Barsoum Z, Jonsson B. Fatigue assessment and LEFM analysis of cruciform joints fabricated with different welding processes. Weld World 2008;52(7):93–105.
- [83] Schubnell J, Jung M, Le CH, Farajian M, Braun M, Ehlers S, Fricke W, Garcia M, Nussbaumer A, Baumgartner J. Influence of the optical measurement technique and evaluation approach on the determination of local weld geometry parameters for different weld types. Weld World 2020;64(2):301–16.
- [84] Hultgren G, Myrén L, Barsoum Z, Mansour R. Digital scanning of welds and influence of sampling resolution on the predicted fatigue performance: modelling, experiment and simulation. Metals 2021;11(5):822.
- [85] Sherry A, Sanderson D, Lidbury D, Ainsworth R, Kikuchi K. The application of local approach to assess the influence of in-plane constraint on cleavage fracture. In: ASME pressure vessels and piping conference 304. ASME; 1995, p. 495–501
- [86] Muhammed A, Pisarski HG, Stacey A. Using wide plate test results to improve predictions from probabilistic fracture mechanics. In: 13 th European conference on fracture. ECF, 2000, p. 6–9.
- [87] Maljaars J, Rózsás Á, Walters CL, Slot H. Uncertainty quantification of the failure assessment diagram for flawed steel components in BS 7910: 2019. Eng Fract Mech 2022;268:108446.
- [88] Altamura A, Straub D. Reliability assessment of high cycle fatigue under variable amplitude loading: Review and solutions. Eng Fract Mech 2014;121:40–66.
- [89] Anderson TL. Fracture mechanics: fundamentals and applications. Boca Raton: Taylor and Francis; 2005.
- [90] Souza G, Ayyub B. Probabilistic fatigue life prediction for ship structures using fracture mechanics. Nav Eng J 2000;112(4):375–97.
- [91] Lukić M, Cremona C. Probabilistic assessment of welded joints versus fatigue and fracture. J Struct Eng 2001;127(2):211–8.
- [92] Ayala-Uraga E, Moan T. Fatigue reliability-based assessment of welded joints applying consistent fracture mechanics formulations. Int J Fatigue 2007;29(3):444–56.
- [93] Doshi K, Roy T, Parihar YS. Reliability based inspection planning using fracture mechanics based fatigue evaluations for ship structural details. Mar Struct 2017;54:1–22.
- [94] Bowness D, Lee M. Fracture mechanics assessment of fatigue cracks in offshore tubular structures. HSE offshore technology report 2000/077, Health and Safety Executive: 2002.
- [95] Dijkstra O, Snijder H, Van Straalen I.J. Fatigue crack growth calculations using stress intensity factors for weld toe geometries. In: Salama M, editor. Proc. 8th int. conf. on offshore mechanics and artic eng.. 1989, p. 137–44.
- [96] Hensel J, Nitschke-Pagel T, Dilger K. Engineering model for the quantitative consideration of residual stresses in fatigue design of welded components. Weld World 2017;61(5):997–1002.
- [97] DNV GL. Fatigue design of offshore steel structures. DNV GL AS; 2021, DNV-RP-C203.
- [98] Leander J, Norlin B, Karoumi R. Reliability-based calibration of fatigue safety factors for existing steel bridges. J Bridge Eng 2015;20:04014107.
- [99] ISO. Petroleum and natural gas industries Floating offshore structures Part 1: Ship-shaped, semi-submersible, spar and shallowdraught cylindrical structures. International Organization for Standardization (ISO); 2019, EN ISO 19904-1:2019.
- [100] Miles JW. On structural fatigue under random loading. J Aeronaut Sci 1954;21(11):753–62.
- [101] Lutes LD, Sarkani S. Random vibrations analysis of structural and mechanical systems. Elsevier Inc.: 2004.
- [102] IEC. Wind energy generation systems Part 3-2: Design requirements for floating offshore wind turbines. International Electrotechnical Commission (IEC); 2019, IEC TS 61400-3-2:2019.
- [103] Matsuishi M, Endo T. Fatigue of metals subjected to varying stress. 1968, Paper presented to Japan Society of Mechanical Engineers Jukvoka.
- [104] Amzallag C, Gerey JP, Robert JL, Bahuaud J. Standardization of the rainflow counting method for fatigue analysis. Int J Fatigue 1994;16(4):287–93.
- [105] ASTM. Standard practices for cycle counting in fatigue analysis. West Conshohocken, PA: ASTM International; 2017, ASTM E1049-85.
- [106] Veldkamp HF. Chances in wind energy a probabilistic approach to wind turbine fatigue design (Ph.D. thesis), Delft University of Technology; 2006, 90-76468-12-5.

[107] Pierson Jr WJ, Moskowitz L. A proposed spectral form for fully developed wind seas based on the similarity theory of S. A. Kitaigorodskii. J Geophys Res (1896-1977) 1964:69(24):5181–90.

- [108] ISO. Petroleum and natural gas industries Specific requirements for offshore structures – Part 1: Metocean design and operating considerations. International Organization for Standardization (ISO); 2015, EN ISO 19901-1:2015.
- [109] Hasselmann K, Barnett T, Bouws E, Carlson H, Cartwright D, Enke K, Ewing J, Gienapp H, Hasselmann D, Kruseman P, Meerburg A, Muller P, Olbers D, Richter K, Sell W, Walden H. Measurements of wind-wave growth and swell decay during the joint north sea wave project (JONSWAP). Dtsch Hydrogr Z 1973:8:1–95.
- [110] Nordenström N. A method to predict long-term distributions of waves and waveinduced motions and loads on ships and other floating structures. Det Norske Veritas (DNV): 1973. Report 81.
- [111] Li L, Gao Z, Moan T. Joint distribution of environmental condition at five European offshore sites for design of combined wind and wave energy devices. J Offshore Mech Arct Eng 2015;137(3).
- [112] IEC. Wind energy generation systems Part 1: Design requirements. International Electrotechnical Commission (IEC); 2019, IEC 61400-1:2019.
- [113] Kaimal JC, Wyngaard JC, Izumi Y, Coté OR. Spectral characteristics of surface-layer turbulence. Q J R Meteorol Soc 1972;98(417):563–89.
- [114] CEN. Eurocode 1: Actions on structures Part 2: Traffic loads on bridges. European Committee for Standardization (CEN); 2003, EN 1991-2:2003.
- [115] Jacob B, O'Brien EJ. Weigh-in-motion: Recent developments in Europe. In: Jacob B, Gonzalez A, Chou C-p, editors. Proceedings of the 4th international conference on WIM. ICWIM4, National University of Taiwan; 2005, p. 1–11.
- [116] Moses F. Weigh-in-motion system using instrumented bridges. Transp Eng J ASCE 1979;105(3):233–49.
- [117] Sedlacek G, Merzenich G, Paschen M, Bruls A, Sanpaolesi L, Croce P, Calgaro J, Pratt M, Leendertz M, de Boer V, Vrouwenvelder A, Hanswille G. Background document to EN 1991: Part 2 Traffic loads for road bridges and consequences for the design. JRC Scientific and Technical Reports; 2008.
- [118] Croce P. Background to fatigue load models for eurocode 1: Part 2 traffic loads. Prog Struct Eng Mater 2001;3(4):335–45.
- [119] Laman JA, Nowak AS. Fatigue-load models for girder bridges. J Struct Eng 1996:122(7):726–33.
- [120] Maljaars J. Evaluation of traffic load models for fatigue verification of European road bridges. Eng Struct 2020;225.
- [121] Leander J. Reliability evaluation of the eurocode model for fatigue assessment of steel bridges. J Constr Steel Res 2018;141:1–8.
- [122] D'Angelo L, Nussbaumer A. Reliability based fatigue assessment of existing motorway bridge. Struct Saf 2015;57:35–42.
- [123] Maddah N. Fatigue life assessment of roadway bridges based on actual traffic loads (Ph.D. thesis), Lausanne: EPFL; 2013, Thèse No 5575.
- [124] Guo T, Frangopol DM, Chen Y. Fatigue reliability assessment of steel bridge details integrating weigh-in-motion data and probabilistic finite element analysis. Comput Struct 2012:112–113:245–57.
- [125] Chotickai P, Bowman MD. Truck models for improved fatigue life predictions of steel bridges. J Bridge Eng 2006;11(1):71–80.
- [126] Szerszen MM, Nowak AS, Laman JA. Fatigue reliability of steel bridges. J Constr Steel Res 1999;52(1):83–92.
- [127] Hellebrandt L, Blom CBM, Steenbergen RDJM. Probabilistic traffic load model for shortspan city bridges. Heron 2014;59(2–3):147–68.
- [128] Kalin J, Žnidarič A, Anžlin A, Kreslin M. Measurements of bridge dynamic amplification factor using bridge weigh-in-motion data. Struct Infrastruct Eng 2021;1–13. http://dx.doi.org/10.1080/15732479.2021.1887291.
- [129] CEN. Railway applications Line categories for managing the interface between load limits of vehicles and infrastructure. European Committee for Standardization (CEN); 2021, EN 15528:2021.
- [130] Imam BM, Righiniotis TD, Chryssanthopoulos MK. Probabilistic fatigue evaluation of riveted railway bridges. J Bridge Eng 2008;13(3):237–44.
- [131] Tobias DH, Foutch DA, Choros J. Loading spectra for railway bridges under current operating conditions. J Bridge Eng 1996;1(4):127–34.
- [132] Rakoczy AM, Liu S, Otter D, Dick S. Current loading spectra for evaluation of railway bridges. Transportation Technology Center, Inc. (TTCI); 2018, Technology Digest TD-18-019.
- [133] James G. Analysis of traffic load effects on railway bridges (Ph.D. thesis), Stockholm: KTH Royal Institute of Technology; 2003, TRITA-BKN. Bulletin 70.
- [134] Tobias DH. A method for the fatigue evaluation of riveted steel girder railway bridges (Ph.D. thesis), University of Illinois at Urbana-Champaign; 1994.
- [135] Musser DW. Summary of tests on steel girder spans. In: Proceedings of the fifty-ninth annual convention of the American railway engineering association. Vol. 61, 1960, p. 51–78.
- [136] Maljaars J, Leonetti D, Hashemi B, Snijder HB. Systematic derivation of safety factors for the fatigue design of steel bridges. Struct Saf 2022;97.
- [137] Tarp-Johansen NJ. Partial safety factors and characteristic values for combined extreme wind and wave load effects. J Solar Energy Eng 2005;127(2):242–52.
- [138] Sørensen JD. Reliability-based calibration of fatigue safety factors for offshore wind turbines. Int J Offshore Polar Eng 2012;22(3):234–41.

[139] Márquez-Domínguez S, Sørensen JD. Fatigue reliability and calibration of fatigue design factors for offshore wind turbines. Energies 2012;5(6):1816–34.

- [140] Road Directorate. Reliability-based classification of the load bearing capacity of existing bridges. Guideline document (in Danish), 2004. Report 291.
- [141] Jacob B, O'Brien E, Jehaes S. Weigh-in-motion of road vehicles: final report COST 323. COST; 2002.
- [142] Straub D, Schneider R, Bismut E, Kim H-J. Reliability analysis of deteriorating structural systems. Struct Saf 2020;82:101877.
- [143] Rackwitz R, Fiessler B. Structural reliability under combined load sequences. Comput Struct 1978;9:489–94.
- [144] Beck AT, Melchers RE. Overload failure of structural components under random crack propagation and loading–a random process approach. Struct Saf 2004;26(4):471–88.
- [145] Fisher JW, Wright W, Sivakumar B, Kaufmann EJ, Xi Z, Edberg W, Tjiang H, Center A. Hoan bridge forensic investigation failure analysis final report. Tech. rep., Wisconsin Department of Transportation; 2001.
- [146] No names. Highway accident report collapse of a suspended span of interstate route 95 highway bridge over mainus river, greenwich, connecticut, June 8, 1983. National Transportation Safety Board; 1984.
- [147] Straub D, Der Kiureghian A. Reliability acceptance criteria for deteriorating elements of structural systems. J Struct Eng Trans ASCE 2011;137(12):1573–82.
- [148] Moan T. Reliability-based management of inspection, maintenance and repair of offshore structures. Struct Infrastruct Eng 2005;1(1):33–62.
- [149] Straub D, Havbro Faber M. Risk based acceptance criteria for joints subject to fatigue deterioration. J Offshore Mech Arct Eng 2004;127(2):150–7. http: //dx.doi.org/10.1115/1.1894412.
- [150] Mendoza J, Nielsen JS, Sørensen JD, Köhler J. Structural reliability analysis of offshore jackets for system-level fatigue design. Struct Saf 2022;97:102220.
- [151] Haghani R, Al-Emrani M, Heshmati M. Fatigue-prone details in steel bridges. Buildings 2012;2(4):456–76.
- [152] ECCS TC 6. Background information on fatigue design rules. Statistical evaluation. Background documentation 9.01 (2nd edition). Brussels: ECCS; 2018.
- [153] Moses C, Raju K. Fatigue evaluation procedures for steel bridges. NCHRP report 299, Highway Research Board; 1987.
- [154] 1990:2005 E. Eurocode basis of structural design. CEN; 2005.
- [155] Sørensen JD. Framework for risk-based planning of operation and maintenance for offshore wind turbines. Wind Energy 2009;12(5):493–506.
- [156] DIN. DIN 15018: Cranes. Steel structures. Berlin: German Standards Organisation; 1974.
- [157] Institution BS. BS 5400:1980 Steel, concrete and composite bridges. British Standards Institution BSI; 1980.
- [158] Fisher J. Guide to 1974 AASHTO fatigue specifications. American Institute of Steel Construction; 1974.
- [159] Gurney T. A re-analysis of fatigue data for welding joints in steel. Weld Res Int 1973;3:1–54.
- [160] 6 ETC. Recommendations for the fatigue design of steel structures, publication no 43. Brussels: European Convention for Constructional Steelwork; 1985.
- [161] Drebenstedt K, Euler M. Statistical analysis of fatigue test data according to eurocode 3. In: Powers, Frangopol, Al-Mahaidi, Caprani, editors. Proceedings of maintenance, safety, risk, management and life-cycle performance of bridges. NCRC Press; 2018, p. 2244–51.
- [162] Hobbacher A. Recommendations for fatigue design of welded joints and components, vol. 47, Springer; 2016.
- [163] prEN 1993-1-9:2023. Eurocode 3: design of steel structures part 1-9: fatigue (formal vote version). CEN: 2023.
- [164] Rausand M, Hoyland A. System reliability theory: models, statistical methods, and applications, vol. 396, John Wiley & Sons; 2003.
- [165] Han X, Frangopol DM. Fatigue reliability analysis considering corrosion effects and integrating SHM information. Eng Struct 2022;272:114967.
- [166] Jeong Y, Kim W, Lee I, Lee J. Bridge inspection practices and bridge management programs in China, Japan, Korea, and US. J Struct Integr Maint 2018;3(2):126–35.
- [167] Tang WH. Probabilistic updating of flaw information. J Test Eval 1973;1(6):459–67.
- [168] Madsen H. Model updating in reliability theory. In: Proc. ICASP5. Vancouver Canada; 1987, p. 565–77.
- [169] Straub D. Reliability updating with equality information. Probab Eng Mech 2011;26(2):254–8.
- [170] Bismut E, Straub D. A unifying review of NDE models towards optimal decision support. Struct Saf 2022;97:102213.
- [171] Hovey PW, Berens AP. Statistical evaluation of NDE reliability in the aerospace industry. In: Review of progress in quantitative nondestructive evaluation. Springer; 1988, p. 1761–8.
- [172] Schneider CR, Rudlin JR. Review of statistical methods used in quantifying NDT reliability. Insight-Non-Destruct Test Cond Monit 2004;46(2):77–9.
- [173] Moan T, Vårdal OT, Hellevig N-C, Skjoldli K. Initial crack depth and POD values inferred from in-service observations of cracks in North Sea jackets. J Offshore Mech Arct Eng 2000;122(3):157–62.

- [174] Rudlin J, Dover W. The ICON project data for underwater inspection. Insight 1996;38(6):412–4.
- [175] Straub D. Generic approaches to risk based inspection planning for steel structures (Ph.D. thesis), ETH Zürich; 2004.
- [176] Spencer Jr B, Tang J. Markov process model for fatigue crack growth. J Eng Mech 1988;114(12):2134–57.
- [177] Rastogi R, Ghosh S, Ghosh A, Vaze K, Singh P. Fatigue crack growth prediction in nuclear piping using Markov chain Monte Carlo simulation. Fatigue Fract Eng Mater Struct 2017;40(1):145–56.
- [178] Yang J-N, Trapp W. Inspection frequency optimization for aircraft structures based on reliability analysis. J Aircr 1975;12(5):494–6.
- [179] Faber MH, Engelund S, Sørensen JD, Bloch A. Simplified and generic risk based inspection planning. In: 19th international conference on offshore mechanics and arctic engineering. 2000.
- [180] Straub D, Faber MH. Risk based inspection planning for structural systems. Struct Saf 2005;27(4):335–55.
- [181] Bismut E, Straub D. Optimal adaptive inspection and maintenance planning for deteriorating structural systems. Reliab Eng Syst Saf 2021;215:107891.
- [182] Morato PG, Andriotis CP, Papakonstantinou KG, Rigo P. Inference and dynamic decision-making for deteriorating systems with probabilistic dependencies through Bayesian networks and deep reinforcement learning. Reliab Eng Syst Saf 2023;235:109144.
- [183] Mendoza J, Bismut E, Straub D, Köhler J. Optimal life-cycle mitigation of fatigue failure risk for structural systems. Reliab Eng Syst Saf 2022;222:108390.